Secretory kinase FAM20C triggers adipocyte dysfunction inciting insulin

2 resistance and inflammation in obesity

- 3 Authors: Ankit Gilani¹, Benjamin Stein^{2,#}, Anne Hoffman³, Renan Pereira de Lima¹,
- 4 Elizabeth E. Ha¹, Edwin A. Homan¹, Lunkun Ma¹, Alfonso Rubio-Navarro¹, Tint Tha Ra
- 5 Wun¹, Gabriel Jose Ayala Carrascal¹, Bhavneet Bhinder⁵, Adhideb Ghosh⁶, Falko Noé⁶,
- 6 Olivier Elemento⁵, Christian Wolfrum⁶, Matthias Blüher^{5,7}, James C. Lo^{1*}

7 Affiliations:

1

- ¹Division of Cardiology, Department of Medicine, Weill Center for Metabolic Health,
- 9 Cardiovascular Research Institute, Weill Cornell Medicine; New York, New York.
- ²Department of Medicine, Weill Cornell Medicine; New York, New York.
- ³Helmholtz Institute for Metabolic, Obesity and Vascular Research (HI-MAG) of the
- 12 Helmholtz Center Munich at the University of Leipzig and University Hospital Leipzig:
- 13 Leipzig, Germany.
- ⁵Englander Institute of Precision Medicine, Weill Cornell Medicine; New York, New York.
- 15 6Institute of Food, Nutrition and Health; ETH Zurich, 8092 Schwerzenbach, Switzerland
- ⁷Medical Department III Endocrinology, Nephrology, Rheumatology, University of
- 17 Leipzig Medical Center; Leipzig, Germany
- [#]Present address: Biological Sciences Division, University of Chicago; Chicago, Illinois,
- 19 60637.
- ^{*}Address correspondence to: James C. Lo, 413 East 69th St., New York, New York,
- 21 10021, USA. Phone: 646.962.2038; Email: jlo@med.cornell.edu.

Conflict-of-interest statement:

- MB received honoraria as a consultant and speaker from Amgen, AstraZeneca, Bayer,
- 24 Boehringer-Ingelheim, Lilly, Novo Nordisk, Novartis, and Sanofi. TE received honoraria
- as a consultant and speaker from Bayer, Boehringer Ingelheim, Fresenius Medical Care,
- Lilly, Novo Nordisk, Sanofi, and Santis. All other authors declare no competing financial
- interests related to this work.

22

Abstract:

29

30

31

32

33

34

35

36

37

38

39

40

41

42

43

44

45

46

47

48

49

Obesity is a major driver of type 2 diabetes (T2D) and related metabolic disorders, characterized by chronic inflammation and adipocyte dysfunction. However, the molecular triggers initiating these processes remain poorly understood. We identify FAM20C, a serine/threonine kinase, as an early obesity-induced mediator of adipocyte dysfunction. Fam20c expression is substantially upregulated in adipocytes in response to obesity, correlating with a proinflammatory transcriptional signature. Forced expression of Fam20c in adipocytes promotes robust upregulation of proinflammatory cytokines and induces insulin resistance that is dependent on its kinase activity. Conversely, deletion of adipocyte Fam20c after established obesity and hyperglycemia improves glucose tolerance, augments insulin sensitivity, and reduces visceral adiposity, without altering body weight. Phosphoproteomic studies reveal that FAM20C regulates phosphorylation of intracellular and secreted proteins, modulating pathways critical to inflammation, metabolism, and extracellular matrix remodeling. We identify FAM20C-dependent substrates, such as CNPY4, whose phosphorylation contributes to proinflammatory adipocyte signaling. Of translational relevance, we show that in humans visceral adipose FAM20C expression positively correlates with insulin resistance. Our findings establish FAM20C as an early regulator of obesity-induced adipocyte dysfunction and systemic metabolic impairment. Our studies provide proof of concept that inhibition of FAM20C may serve as a potential therapy for T2D by restoring adipocyte health.

Main Text:

50

51

52

53

54

55

56

57

58

59

60

61

62

63

64

65

66

67

68

69

70

71

72

Introduction

Obesity and type 2 diabetes (T2D) have reached epidemic proportions globally. profoundly impacting public health by increasing the risk for comorbidities including cardiovascular diseases, cancer, kidney and liver dysfunction, and retinal damage (1-4). Central to T2D development is obesity, which induces a cascade of metabolic derangements, notably in adipose tissues (5, 6). Adipocytes regulate metabolism by storing excess energy and releasing adipokines that control insulin sensitivity and inflammation (6, 7). However, obesity induces a state of adipocyte dysfunction involving increased production of pro-diabetic adipokines such as RBP4, decreased secretion of the anti-diabetic adipokines adiponectin and adipsin, insulin resistance, release of toxic metabolites, diminished thermogenic capacity, and chronic inflammation (8-15). Although adipocyte dysfunction is a known driver of obesity-associated metabolic diseases such as T2D, the molecular mediators initiating this process remain poorly understood. Kinases such as c-Jun NH2-terminal kinase (JNK)(16), noncanonical IkB kinases including IkB kinase epsilon (IKKε) and TANK-binding kinase 1 (TBK) (17-19) have been implicated in adipocyte inflammation and insulin sensitivity, highlighting a critical role of protein phosphorylation in development of adipocyte dysfunction.

Family with sequence similarity 20, member C (FAM20C) also known as Dentin Matrix Protein 4 (DMP4) is a Golgi-localized and secreted serine/threonine protein kinase (20). It phosphorylates secretory pathway proteins with S-x-E/pS motifs and regulates biomineralization of bones and teeth (21-23). FAM20C contributes to the extracellular phosphoproteome and is implicated in biological functions such as wound healing (24),

cell adhesion and migration (25-27), endocytosis (28), and lipoprotein receptor binding (29).

Obesity is often associated with hyperglycemia, hypertension, dyslipidemia, and some cancers, which are key features of metabolically unhealthy obesity (MUO). However, a subset of obese individuals, termed metabolically healthy obese (MHO), have a substantially lower risk of developing these typical cardiometabolic diseases compared to MUO (30-32). This paradox suggests that adipocyte function plays a critical role in determining whether obesity leads to metabolic dysfunction, rather than the mere accumulation of fat. Adipocyte dysfunction is observed in MUO, whereas MHO maintain better adipocyte function with low inflammation (31, 32), though the underlying mechanisms remain unclear. Identifying molecular mediators initiating the process of adipocyte dysfunction could explain the heterogeneity of cardiometabolic risk factor prevalence in obesity.

Here, we investigate the molecular mechanisms underlying adipocyte dysfunction and identify the kinase FAM20C as a critical regulator of this process. Our data support a model where FAM20C serves as an early mediator of obesity-induced inflammatory signaling and insulin resistance in adipocytes, contributing to the progression from obesity to insulin resistance and T2D. We demonstrate that *Fam20c* expression is upregulated in adipocytes in response to obesity and its kinase activity drives a proinflammatory gene expression signature. Importantly, knockout of *Fam20c* in adipocytes after established obesity and hyperglycemia, corrects glucose intolerance and insulin resistance, suggesting that targeting *Fam20c* could be a potential strategy for restoring adipocyte function and metabolic homeostasis. Our phosphoproteomic studies reveal substrates

and pathways regulated by adipocyte FAM20C that may contribute to its pathophysiological actions. By identifying *Fam20c* as a key molecular switch in adipocyte dysfunction, our findings provide new insights into the mechanisms driving obesity-related metabolic diseases and offer potential therapeutic avenues for preventing or treating T2D.

Results

101

102

103

104

105

106

107

108

109

110

111

112

113

114

115

116

117

118

119

120

121

122

123

Obesity induces Fam20c, a serine threonine kinase, in adipocytes

To identify adipocyte-derived factors that drive early obesity and T2D, we assessed adipose tissue, adipocyte, and stromal vascular fraction (SVF) in the well-established B6 model of diet-induced obesity (Fig. 1A). B6 wild-type (WT) mice were placed on a 60% high fat diet (HFD) or regular chow diet (CD) for 4 weeks. Unbiased transcriptomic analyses on visceral white adipose tissues (WAT) revealed over 200 genes induced in response to obesity (Fig. 1B). Pathway analysis of differentially expressed genes (DEG) revealed enrichment of cholesterol biosynthesis and metabolism, focal adhesion, and PI3K-Akt-mTOR signaling pathways (Fig. S1A). We also performed an unbiased transcriptomic analysis of the adipocyte fraction and the SVF from these mice (Fig. 1C-D). Similar to the whole adipose tissue, pathways associated with focal adhesion and PI3K Akt mTOR signaling were also enriched in the adipocyte fraction (Fig. S1B) whereas pathways for P53 signaling, oxidative stress, and redox pathways were enriched in SVF (Fig. S1C). To identify adipocyte-specific factors that initiate dysfunction, we performed a preliminary screening of the top candidate genes highly induced in adipocytes in obesity. Lentiviral vector transduction of these factors in primary differentiated adipocytes identified Fam20c as a substantial inducer (2-6 fold) of II6 and CcI2 (Fig. 1E), indicating a potential role in promoting adipose inflammation. Beyond its transcriptional effects, Fam20c was prioritized for further study based on its biochemical classification as a secreted protein and a kinase, both categories of proteins previously implicated in adipose inflammation and dysfunction. We found that Fam20c expression was robustly induced early on in obesity (Fig. 1B) and was specific to the adipocyte fraction (Fig. 1C),

as *Fam20c* expression was unchanged in the SVF (Fig. 1D). These data indicate that *Fam20c* is specifically induced in adipocytes within WAT in response to obesity. Figure 1F shows a schematic of mouse FAM20C, a 579-aa protein, with its kinase domain, a putative pro-peptide, a proline rich region, and N-linked glycosylation sites. The kinase domain contains the D473 metal-binding site essential for its enzymatic activity.

124

125

126

127

128

129

130

131

132

133

134

135

136

137

138

139

140

141

142

143

144

145

146

Fam20c expression was 2.5-fold, 3.4-fold, and 2.8-fold higher at 2, 4, and 15 weeks HFD-feeding respectively, indicating an early and sustained induction throughout obesity (Fig. 1G). Fam20c was similarly induced in the subcutaneous WAT and brown adipose tissue (BAT) depots of HFD-fed mice compared to CD (Fig. S1D-E). We also examined basal expression of Fam20c in various tissues from chow-fed WT mice, including BAT, subcutaneous WAT, visceral WAT, bone, heart, muscle, liver, and brain. Expression of Fam20c in adipose depots was comparable to bone, a mineralized tissue previously reported to have high *Fam20c* expression (Fig. S1F) (33). Moreover, *Fam20c* was upregulated in adipose tissues but not in other metabolic tissues such as liver (Fig. S1G-I). It is possible that the increased *Fam20c* in HFD-fed mice results from nutrient composition (e.g., lipid content) of the diet rather than obesity. Visceral WAT of genetically obese ob/ob mice fed a CD demonstrated 5-fold higher adipose Fam20c ob/ob mice compared to WT controls, suggesting that obesity rather than specific dietary factors drives Fam20c induction (Fig. 1H). These findings establish Fam20c as an early obesityinduced kinase expressed in adipocytes.

Given strong induction of *Fam20c* in adipocytes during obesity, we examined whether this regulation was linked to specific adipocyte subpopulations by analyzing single-cell and single-nucleus RNA-seq datasets of mouse and human WAT (34). In mice,

Fam20c was upregulated across all six adipocyte subclusters following HFD, with the strongest induction in mAd1–3 and mAd6 (Fig. S2A). In human WAT, FAM20C expression was substantially enriched in the hAd5 subcluster, and the proportion of hAd5 cells positively correlated with BMI, suggesting an association between FAM20C expression and obesity-driven expansion of specific adipocyte populations (Fig. S2B). Together, these results suggest that Fam20c upregulation is a conserved, obesity-associated feature of specific adipocyte subtypes in both mice and humans.

Fam20c induces a broad proinflammatory gene expression pattern and insulin resistance in adipocytes

We hypothesized that *Fam20c* in adipocytes may promote adipose inflammation and adipocyte dysfunction to trigger metabolic impairment and T2D. To assess the effect of FAM20C kinase in adipocytes, we overexpressed *Fam20c* in primary differentiated adipocytes using adenovirus carrying the mouse *Fam20c* wild-type gene (Fig. 2A and S2C-D). Forced expression of *Fam20c* resulted in a substantial (2- to 6-fold) increase in chemokine and cytokine genes, including *Ccl2*, *Ccl5*, *II1b*, and *Tnf* (Fig. 2B). To ascertain if these effects require FAM20C's kinase activity, we engineered a catalytically inactive mutant (D473A) of FAM20C (Fig. 2A). By contrast, the *Fam20c D473A* mutant did not elicit an increase in chemokine and cytokine expression (Fig. 2B). To determine the full extent of the effects of *Fam20c* on adipocytes, we performed unbiased transcriptomic analyses on primary adipocytes transduced with *Fam20c*. The majority of genes regulated in response to *Fam20c* were related to inflammation, indicating that FAM20C preferentially induces a broad proinflammatory expression pattern (Fig. 2C). Importantly, the kinase activity of FAM20C was necessary for these effects as the kinase dead

FAM20C mutant failed to elicit the same response as the WT (Fig. 2C). Pathway analysis revealed activation of Tnf- α signaling, inflammatory response, and IL-6/JAK/STAT3 pathways (Fig. 2D). Forced expression of *Fam20c* in the L1 adipocyte cell line recapitulated the inflammatory gene expression seen in primary adipocytes (Fig. S2E), supporting a direct cell autonomous role of FAM20C in promoting robust inflammatory gene expression pattern in adipocytes.

Building on the link between *Fam20c* upregulation and adipocyte dysfunction, we investigated whether *Fam20c* directly contributes to insulin resistance. To this end, we performed in vitro insulin sensitivity assays in primary adipocytes overexpressing either wild-type or catalytically inactive *Fam20c*. Overexpression of *Fam20c* in adipocytes caused a striking ~70% reduction in insulin-stimulated Akt phosphorylation compared to GFP control, indicating profound impairment in insulin signaling (Fig. 2E–F). In contrast, the D473A mutant had no effect, indicating that this impairment is dependent on FAM20C's kinase activity. Together, these findings support a direct, kinase-dependent role for FAM20C in promoting adipocyte inflammation and insulin resistance.

Identification of Fam20c-dependent transcriptional changes in adipocytes under physiological condition

To investigate the role of Fam20c in adipocytes, we ablated Fam20c specifically in adipocytes by crossing Fam20c-floxed and Adiponectin-Cre transgenic mice. Primary differentiated adipocytes from control (Fam20c-floxed) and Ad-Fam20c KO (Fam20c floxed/Adiponectin-Cre) mice were subjected to RNA-Seq to identify Fam20c-dependent transcriptional alterations. Analysis of DEGs revealed a significant downregulation of 63 and upregulation of 5 transcripts in the KO adipocytes (Fig. 2G). Pathway enrichment

analysis revealed suppression of pathways linked to adipocyte dysfunction, including epithelial-mesenchymal transition, apical junction assembly, KRAS signaling, and inflammatory response, whereas pathways associated with enhanced adipocyte function, including fatty acid metabolism, adipogenesis, and oxidative phosphorylation, were upregulated in the adipocytes devoid of *Fam20c* (Fig. 2H). Adipocyte dysfunction is often associated with an imbalance of adipokine secretion leading to inflammation and insulin resistance. To determine whether *Fam20c* regulates the adipocyte secretome, we filtered for genes encoding secreted proteins or extracellular space components. Among these, *Esm1* (endothelial cell-specific molecule 1) exhibited the most significant downregulation in KO adipocytes (Fig. S2F). *Esm1* regulates fatty acid synthesis, cell migration, integrin binding, and angiogenesis (35, 36), suggesting that its decreased expression in KO adipocytes may correspond to reduced immune cell infiltration and inflammation. Expression of several proinflammatory cytokines (*Ccl6*, *Ccl8*, *Cxcl16*, and *ll16*) was also reduced in the KO adipocytes (Fig. S2G).

Upstream analysis revealed activation of transcription factors associated with improved adipocyte metabolism in KO adipocytes. PPARGC1A was notably activated, a key regulator of adipose tissue metabolism and thermogenesis (37) (Fig. 2I). Conversely, transcription factors linked to cell growth and inflammatory signaling, such as RICTOR and WNT3A, were inactivated. Upstream cytokine analysis showed substantial inactivation of proinflammatory cytokines such as TNF, CCL2, and CCL20 in KO adipocytes (Fig. 2J). Remarkably, NAMPT, a cytokine associated with improved insulin sensitivity in adipose tissue (38), was upregulated in the KO group. These findings suggest that under physiological conditions, adipocyte *Fam20c* drives the activation of

proinflammatory cytokines and chemokines, while repressing transcription factors and cytokines linked to enhanced adipocyte function and insulin sensitivity.

Adipocyte-specific knockout of *Fam20c* in obese and diabetic mice improves glucose metabolism and insulin sensitivity

To investigate the pathophysiological role of adipocyte *Fam20c*, we generated constitutive (Ad-Fam20c KO) and inducible (iAd-Fam20c KO) adipocyte-specific *Fam20c* knockout mice by crossing *Fam20c-floxed* with *Adiponectin-Cre* and *Adiponectin-CreERT* transgenic lines, respectively. Under CD, neither model exhibited significant metabolic alterations. In Ad-Fam20c KO mice, body weight and glucose tolerance were comparable to controls (Fig. S3A–B). Similarly, in iAd-Fam20c KO mice, in which *Fam20c* deletion was induced in 12-week-old adults, body weight and glucose tolerance remained unchanged relative to controls (Fig. S3C–D). Furthermore, the weights of major metabolic tissues, including BAT, subcutaneous and visceral WAT depots, and liver, were not different between groups (Fig. S3E).

To determine the potential of FAM20C inhibition as a disease modifying therapy for T2D, control and iAd-Fam20c KO mice were fed HFD for 3 months to induce obesity and insulin resistance. Subsequently, tamoxifen was administered to selectively ablate adipocyte Fam20c (Fig. 3A and S3F-G). Following acute Fam20c deletion (2 weeks post injection), body weights were not significantly different between the groups (39.4±3.5g vs.38.6±3.5g for controls) (Fig. 3B). Acute deletion of Fam20c significantly improved glucose tolerance in iAd-Fam20c KO mice compared to controls (Fig. 3C-D). Additionally, insulin tolerance tests (ITT) revealed that iAd-Fam20c KO mice displayed enhanced insulin sensitivity relative to controls (Fig. 3E-F). These findings suggest that acute

deletion of adipocyte *Fam20c* ameliorates glucose homeostasis and insulin resistance in the context of diet-induced obesity.

239

240

241

242

243

244

245

246

247

248

249

250

251

252

253

254

255

256

257

258

259

260

261

To further evaluate for sustained effects of adipocyte Fam20c deletion on glucose metabolism, we extended the study to determine longer term effects of FAM20C disruption. Control and iAd-Fam20c KO mice were maintained on HFD for an additional 12 weeks with monthly tamoxifen injections to maintain *Fam20c* KO (Fig. 3A). Although body weight was not changed (Fig. 3G), chronic deletion of adipocyte Fam20c continued to confer substantial metabolic benefits. Both glucose tolerance and insulin sensitivity continued to improve by ~25% and >100%, respectively, compared to controls (Fig. 3H-K). These results indicate that the therapeutic benefits of adipocyte *Fam20c* deletion on glucose metabolism and insulin sensitivity are sustained over an extended period of metabolic stress. Additionally, we assessed adipose tissue insulin sensitivity using the adipo-IR index, which integrates plasma free fatty acids (FFA) and insulin. The adipo-IR index was ~40% lower in iAd-Fam20c KO mice compared to controls (0.75±0.04 vs. 1.24±0.46, *P*=0.03), suggesting that *Fam20c* deletion ameliorates adipose tissue insulin resistance (Fig. 3L). Taken together, these data support the hypothesis that adipocyte Fam20c deletion enhances glucose metabolism and insulin sensitivity, providing a potential therapeutic avenue for improving metabolic function in established T2D.

Adipocyte-specific knockout of Fam20c results in a reduction of visceral white adipose tissue mass

To assess the impact of adipocyte *Fam20c* deletion on body composition, we conducted metabolic and histological analyses in control and iAd-*Fam20c* KO mice with chronic *Fam20c* deletion. EchoMRI revealed that iAd-*Fam20c* KO mice exhibited a mild

but significant increase in lean mass (27.3±0.4 vs. 26±0.4g, P=0.04) compared to controls, while total fat mass was unchanged (14.7±1.5 vs. 17.2±1.3g, P=0.25), suggesting a redistribution of body mass (Fig. 3M). Consistent with this, the fat-to-lean mass ratio was significantly lower in iAd-Fam20c KO mice (0.55±0.07 vs. 0.74±0.11, P=0.02 for controls), indicating a decrease in overall adiposity relative to lean tissue (Fig. 3N). Additionally, iAd-Fam20c KO mice displayed a striking 40% selective reduction in visceral WAT mass compared to controls, with no significant differences observed in BAT or subcutaneous WAT (Fig. 3O). To investigate whether the observed reduction in visceral WAT mass was associated with changes in adipocyte morphology, we performed histological analysis of H&E-stained sections (Fig. 4A). While the average adipocyte diameter was unchanged (Fig. 4B), frequency distribution analysis revealed a significant shift in adipocyte size distribution. Specifically, iAd-Fam20c KO mice exhibited a significantly higher proportion of smaller adipocytes, and a correspondingly lower proportion of larger adipocytes (Fig. 4C). This shift in adipocyte size distribution likely contributes to the reduced visceral WAT mass. To assess for adipose inflammation, we stained for macrophage markers and quantified crown-like structures (CLS) in the visceral WAT. Numbers of adipose tissue macrophages and CLS were not different between control and iAd-Fam20c KO mice (Fig. S4A-C), indicating that chronic Fam20c deletion following HFD-feeding may not be sufficient to reverse CLS formation and associated proinflammatory changes.

262

263

264

265

266

267

268

269

270

271

272

273

274

275

276

277

278

279

280

281

282

283

284

Collectively, these findings demonstrate that *Fam20c* regulates visceral WAT expansion and adipocyte size distribution, and its deletion offers a protective effect against visceral adiposity and obesity-induced insulin resistance.

Adipocyte Fam20c promotes early inflammatory remodeling and insulin resistance during diet-induced obesity

To define the contribution of adipocyte *Fam20c* to immune cell infiltration during early obesity, we disrupted adipocyte FAM20C after 4 weeks of HFD using inducible iAd-Fam20c KO and control mice. Masses of adipose tissue depots and livers remained unchanged between control and iAd-Fam20c KO mice (Fig. S4D). However, flow cytometric analysis of visceral WAT SVF revealed a 25% reduction in F4/80+CD11b+ adipose tissue macrophages (ATM) in iAd-Fam20c KO mice compared to controls (Fig. 4D and S4E). Visceral WAT tissue B-cells, CD4+, and CD8+ cells were unchanged between the groups (Fig. 4D). Consistent with this, immunohistochemistry of visceral WAT revealed that iAd-Fam20c KO mice had 49% lower macrophage area and 44% lower CLS compared to controls (Fig. 4E-G). These results indicate that adipocyte FAM20C facilitates early macrophage infiltration and proinflammatory remodeling of visceral WAT during obesity onset.

We next examined whether *Fam20c* influences insulin signaling in peripheral tissues during early obesity. Control and iAd-Fam20c KO mice received HFD for 4 weeks followed by acute *Fam20c* deletion and then challenged in vivo with insulin. Insulinstimulated Akt phosphorylation (p-Akt Ser473) was measured in subcutaneous and visceral WAT, liver, and skeletal muscle (Fig. 4E-J). Early and acute adipocyte ablation of *Fam20c* in the course of obesity resulted in substantial improvements in insulin signaling with elevations in insulin-stimulated p-Akt by 1.6 fold in subcutaneous WAT, 1.5 fold in visceral WAT, 1.9 fold in liver, and 2.9 fold in skeletal muscle compared to controls, indicating enhanced insulin responsiveness in multiple metabolic tissues (Fig. 4E-J).

Together, these findings suggest that *Fam20c* facilitates early adipose inflammation and systemic insulin resistance during the initial stages of diet-induced obesity.

308

309

310

311

312

313

314

315

316

317

318

319

320

321

322

323

324

325

326

327

328

329

330

FAM20C regulates phosphorylation of intracellular and secreted proteins in adipocytes, modulating inflammatory and metabolic pathways

FAM20C is a serine/threonine kinase localized to the Golgi apparatus that phosphorylates secreted proteins (21). Since the kinase dead D473A mutant of FAM20C did not elicit an inflammatory gene expression phenotype, we hypothesized that FAM20C actions in adipocytes are mediated via protein phosphorylation. We performed unbiased phosphoproteomics on primary adipocytes transduced with either Fam20c WT, the kinase-dead mutant (D473A), or a control (Gfp) virus (Fig. 5A). Forced expression of Fam20c WT led to the identification of a distinct set of >500 phosphorylated peptides, which were absent in cells overexpressing the Fam20c D473A mutant, confirming kinasedependent nature of these phosphopeptides (Fig. 5B). Motif analysis revealed that majority of these phosphosites exhibited a S-x-E consensus sequence, a known motif specifically targeted by FAM20C among secretory pathway kinases (Fig. 5C). Pathway enrichment analysis of FAM20C-regulated phosphopeptides identified involvement of focal adhesion, PI3K Akt mTOR signaling, and inflammatory response pathways (Fig. 5D), implicating FAM20C regulates key processes involved in cellular metabolism, immune response, and protein trafficking in adipocytes.

Next, to explore the role of FAM20C in modulating phosphorylation of adipocyte secretome, we conducted phosphoproteomics on conditioned media of primary differentiated adipocytes derived from control and Ad-*Fam20c* KO mice (Fig. 6A). Secreted phosphopeptides enriched by Fam20c included LAMA4-Ser283/Ser949,

FGF23-Ser212, FN1-Ser2475, and COL4A2-Ser708, all extracellular matrix (ECM) proteins implicated in fibrosis (Fig. 6B). Most sites conformed to the FAM20C consensus motif of S-x-E (Fig. 6C). Pathway analysis of these secreted phosphopeptides also revealed enrichment of focal adhesion, PI3K-Akt-mTOR, and integrin signaling (Fig. 6D). These findings suggest that FAM20C-mediated phosphorylation regulates the secretion of ECM proteins and signaling molecules that contribute to adipocyte dysfunction, potentially through mechanisms linked to fibrosis and inflammation. Additionally, we observed that FAM20C phosphorylated Patatin-like phospholipase domain-containing protein 2 (PNPLA2, also known as ATGL) at Ser468 (Fig. 6B). PNPLA2 plays a pivotal role in the initiation of triglyceride hydrolysis, suggesting that FAM20C may regulate adipocyte lipolysis through PNPLA2. To investigate the impact of FAM20C on adipose lipolysis, we conducted an ex vivo lipolysis assay using visceral WAT explants from either control or Ad-Fam20c KO mice after 8 weeks of HFD. Basal release of FFA and glycerol was reduced by ~45% and 50%, respectively, in KO explants compared to controls, consistent with improved metabolic regulation following Fam20c deletion (Fig. 6E-H). Stimulation with the β3-adrenoceptor agonist CL-316,243 (0.5 μM) induced similar lipolytic responses in both groups (Fig. 6E-H). These findings are consistent with the established observation that obesity is associated with elevated basal lipolysis due to blunted anti-lipolytic effect of insulin and catecholamine resistance (39-41). Our results suggest that ablation of adipocyte FAM20C reduces basal lipolysis in obesity, likely due to improved insulin sensitivity, without affecting catecholamine responsiveness.

331

332

333

334

335

336

337

338

339

340

341

342

343

344

345

346

347

348

349

350

351

352

353

Together, these data provide strong evidence that FAM20C is a critical kinase in adipocytes, influencing both intracellular and secreted protein phosphorylation. By

regulating key pathways involved in focal adhesion, PI3K/AKT/mTOR signaling, inflammatory response, and lipolysis, FAM20C modulates adipocyte function and contributes to insulin resistance in obesity.

Obesity-induced Fam20c in the visceral WAT phosphorylates proteins involved in adipogenesis and adipose tissue dysfunction

To identify pathological substrates of FAM20C in vivo, we performed phosphoproteomics on visceral WAT of control and Ad-*Fam20c* KO mice on a HFD for 8 weeks to increase FAM20C expression in controls (Fig. 7A). This experimental setup generated a high signal-to-noise ratio, allowing comprehensive assessment of FAM20C's role in adipose tissue dysfunction during obesity. A volcano plot revealed significant changes in phosphorylation patterns between the two groups (Fig. 7B), with most phosphosites conforming to the S-x-E motif, confirming FAM20C specificity (Fig. 7C). Pathway analysis of differentially phosphorylated proteins identified enrichment in integrin mediated cell adhesion, insulin signaling, and regulation of actin cytoskeleton suggesting a critical role for FAM20C in these processes under pathological conditions of obesity (Fig. S5A).

A key substrate of FAM20C identified through phosphoproteomics was Canopy FGF signaling regulator 4 (CNPY4), phosphorylated at Ser64 in a FAM20C-dependent manner (Fig. 7B). CNPY4 is a secreted protein shown to regulate the cell surface expression of Toll-like Receptor-4 (TLR4), which propagates the production of proinflammatory cytokines (42, 43). This prompted us to investigate CNPY4's role in mediating the effect of FAM20C on adipose tissue inflammation. Notably, mouse *Cnpy4* encodes three isoforms and variant-specific qPCR revealed a distinct expression pattern

in visceral WAT during obesity. Isoform 2 was markedly upregulated, isoform 1 was downregulated, and isoform 3 remained unchanged at low expression levels (Fig. 7D). The obesity-inducible expression of isoform 2 prompted us to focus subsequent mechanistic studies on it. To test the hypothesis that CNPY4 phosphorylation by FAM20C promotes inflammation, we overexpressed CNPY4 WT and CNPY4 S64A mutant in primary differentiated adipocytes (Fig. 7E and S5B-C). Adipocytes overexpressing CNPY4 WT exhibited a significant increase in expression of proinflammatory cytokines including *Tnf*, *Il6*, and *Ccl2*, compared to controls (Fig. 7E). In contrast, adipocytes overexpressing the S64A mutant, which lacks the FAM20C phosphorylation site, did not show any increase in inflammatory gene expression of *Tnf and Il6*. *Ccl2* is a FAM20C regulated cytokine but was not regulated by its phosphorylation of CNPY4, indicating that CNPY4 may induce *Ccl2* by FAM20C-independent mechanism. Another FAM20C regulated cytokine *Ccl5* was also unaffected, suggesting CNPY4 mediates part of FAM20C's actions on adipose inflammation.

To investigate whether CNPY4 also mediates insulin resistance downstream of FAM20C, we performed in vitro insulin signaling assays. Following insulin stimulation, primary adipocytes overexpressing WT CNPY4 exhibited significantly reduced Akt phosphorylation (p-Akt Ser473) compared to controls, consistent with impaired insulin signaling (Fig. 7F-G). In contrast, overexpression of the CNPY4 S64A mutant did not impair p-Akt induction by insulin, indicating FAM20C dependent phosphorylation of CNPY4 at Ser64 is required to impair insulin signaling. Taken together, these results suggest that FAM20C-mediated phosphorylation of CNPY4 at Ser64 promotes proinflammatory gene expression and contributes to adipose tissue insulin resistance in

obesity. These findings also highlight the importance of FAM20C in regulating key signaling proteins involved in adipocyte inflammation and dysfunction in obesity.

Adipose FAM20C levels in humans positively correlate to insulin resistance

400

401

402

403

404

405

406

407

408

409

410

411

412

413

414

415

416

417

418

419

420

421

422

To investigate the relationship between FAM20C expression and metabolic dysfunction in humans, we analyzed FAM20C expression in a cross-sectional cohort comprising paired omental (visceral, VIS) and abdominal (subcutaneous, SC) adipose tissues (AT) from 1,480 individuals in the Leipzig Obesity Biobank (LOBB). FAM20C expression was significantly higher in VIS than SC AT in individuals with obesity (Fig. 8A). However, no significant differences in FAM20C were observed between individuals with and without obesity in either VIS or SC AT, though this could be underpowered due to the small number of individuals without obesity (N = 31). We then examined the correlation between FAM20C expression and various metabolic parameters, including body weight, body mass index (BMI), body fat percentage, fasting plasma insulin (FPI), homeostasis model assessment of insulin resistance (HOMA-IR), and HbA1c (Fig. 8B). In both VIS and SC AT, FAM20C levels positively correlated with HOMA-IR, a well-established indicator of insulin resistance (Fig. 8C-D). Additionally, FAM20C expression also showed significant positive correlation with FPI, suggesting a state of hyperinsulinemia in association with insulin resistance (Fig. 8E-F). These findings suggest a potential role for adipose FAM20C in the development of insulin resistance in humans.

In males, *FAM20C* levels in SC AT also correlated positively with body weight and BMI (Fig. 8G-H), suggesting that higher *FAM20C* expression in this depot may be linked to adiposity. To control for the potential confounding effects of antidiabetic medications, we excluded patients receiving glucose lowering treatments, including insulin, metformin,

DPP-4 inhibitors, sulfonylureas, and glitazones (Fig. S6A-B). In this subset, we observed a strong positive correlation between VIS adipose tissue FAM20C levels and both FPI and HOMA-IR (Fig. 8I-J). However, no significant correlations were found for FAM20C levels in SC AT (Fig. S6C-D), further supporting the notion that VIS FAM20C may be a key contributor to the development of insulin resistance in obesity. Taken together, these data suggest that elevated FAM20C in visceral adipose tissue is strongly associated with insulin resistance and hyperinsulinemia in individuals with obesity. In contrast, the correlation between FAM20C and metabolic parameters appears to be weaker in subcutaneous adipose tissue, highlighting specific role of visceral FAM20C in metabolic dysfunction. Visceral adipose remodeling is a hallmark of MUO and is closely linked to adipose tissue dysfunction and systemic insulin resistance. To investigate FAM20C expression in this pathological phenotype, we reanalyzed publicly available singlenucleus RNA-sequencing dataset profiling VAT from individuals with either metabolically healthy or unhealthy obesity (44). Our analysis revealed 60% higher FAM20C expression in visceral adipocytes from MUO individuals compared to MHO counterparts (P = 1.19 × 10⁻¹⁷) (Fig. 8K and S6E). These results identify elevated FAM20C expression as a molecular feature of MUO-associated adipocytes, reinforcing its role in the development of metabolic dysfunction in obesity.

423

424

425

426

427

428

429

430

431

432

433

434

435

436

437

438

439

440

441

DISCUSSION

The global epidemic of obesity and T2D is fueled by a complex pathogenesis involving inflammatory and metabolic disturbances within adipose tissue, particularly adipocyte dysfunction. Despite extensive research on the processes associated with adipocyte dysfunction, critical gaps remain in understanding its molecular triggers. Our study identifies *Fam20c*, an obesity induced gene, as an early mediator of adipocyte dysfunction, unveiling its ability to alter both intracellular and extracellular signaling within adipose tissue. Ablation of adipocyte FAM20C also enhanced insulin sensitivity in other metabolic tissues such as the liver and muscle, placing FAM20C within adipose tissues as a systemic mediator of insulin resistance. By linking FAM20C kinase to adipocyte inflammation, adipose insulin resistance, and systemic metabolic impairment, we expand the current understanding of molecular pathways that transition obesity into T2D, highlighting adipocyte FAM20C as a potential therapeutic target.

A key finding of our study is that *Fam20c* expression is significantly and selectively induced in adipocytes in two mouse models of obesity and T2D with different dietary compositions. This induction is unique to adipocytes, as the SVF did not exhibit a similar upregulation. Prior research has demonstrated cell-type-specific transcriptional responses to metabolic stress in obesity (34, 45). Notably, a single cell study on mouse WAT from Emont *et. al.* revealed *Fam20c* as a marker of an adipocyte subcluster (mAd4) increased with HFD (34). This study also revealed obesity associated increase in *Fam20c* across all six mouse adipocyte subclusters (mAd1-mAd6) and one human adipocyte subcluster (hAd5) that positively correlated with BMI. Sustained induction of *Fam20c* across multiple stages of obesity underscores its potential role as an early and persistent

driver of adipocyte dysfunction. Dietary components of HFD have been shown to influence the degree of metabolic impairment in mouse models (46, 47). The elevation of *Fam20c* in genetically obese *ob/ob* mice, independent of HFD, emphasizes its role as a response to obesity rather than dietary lipid exposure, though it is possible that additional nutritional components may induce *Fam20c*.

Our study further demonstrates that FAM20C's kinase activity is crucial for promoting inflammation and adipocyte dysfunction. Overexpression of wild-type *Fam20c* in primary adipocytes induced a robust proinflammatory gene expression profile and triggered insulin resistance, whereas its kinase-dead mutant (D473A) did not. While other kinases, such as JNK (16, 48) and TBK-1 (17-19), have been implicated in adipose inflammation and dysfunction, these are typically activated by pro-inflammatory cytokine signaling. Notably, TBK-1 can suppress inflammation by attenuating NF-κB (17) and depends on prior adipose inflammation for its activation in obesity (19). In contrast, FAM20C acts as an early mediator of adipocyte dysfunction by directly inducing proinflammatory cytokine signaling, making it a potential target for addressing the initial causes of adipocyte dysfunction.

Pathways linked to TNF-α and IL-6/JAK/STAT3 signaling are well-established contributors to adipose inflammation and systemic insulin resistance (49, 50). Our transcriptomic data from primary adipocytes indicate that *Fam20c* induction upregulates these pathways. Conversely, *Fam20c* knockout leads to downregulation of these pathways and a concomitant upregulation of pathways involved in fatty acid metabolism, adipogenesis, and oxidative phosphorylation. Oxidative phosphorylation is often impaired in obese adipocytes with diminished mitochondrial activity leading to inflammation, insulin

resistance, and adipocyte dysfunction (51, 52). Interestingly, the oxidative phosphorylation pathway was highly activated in *Fam20c* KO adipocytes along with upstream activation of PPARGC1A, a key transcription factor driving mitochondrial biogenesis and thermogenesis. This further supports the notion that *Fam20c* promotes a state of metabolic dysfunction by inhibiting pathways enhancing adipocyte metabolism.

488

489

490

491

492

493

494

495

496

497

498

499

500

501

502

503

504

505

506

507

508

509

510

A recent report showed that mice with constitutive KO of adipocyte Fam20c are protected from diet-induced obesity and have mildly improved glucose homeostasis under HFD (53). With the mild protection from obesity, mild improvements in glucose tolerance were expected in the constitutive adipocyte Fam20c KO. It was unclear if deletion of adipocyte Fam20c can reverse established obesity and T2D. That report also lacked molecular insight into how FAM20C promotes diabetes and obesity. In our study, we used a tamoxifen-inducible model to ablate adipocyte Fam20c after a HFD feeding regimen with similar body weights before and after tamoxifen. We did not observe differences in body weights with post-development deletion of Fam20c, which differs from the other study (53). The basis for the protection from diet-induced obesity remains unknown and could be due to postnatal development issues with adipocyte Fam20c ablation. Importantly, we found that time restricted targeting of adipocyte Fam20c in established T2D remodeled the adipose and enhanced insulin sensitivity. We found no significant changes in the number of ATM or CLS with chronic deletion of adipocyte Fam20c. There may be changes in other immune cell compartments or macrophage subsets with later loss of Fam20C. However, deletion of adipocyte Fam20c following short term HFD decreases ATM populations and CLS, indicating Fam20c promotes inflammatory adipose remodeling during early obesity. Importantly, the improvements in glucose homeostasis

strengthened over three months, suggesting that deletion of *Fam20c* in adipose may be effective as a disease modifying therapy for T2D. These findings highlight that adipocyte-specific *Fam20c* deletion confers sustained metabolic benefits. We also found that adipocyte-specific deletion of *Fam20c* improved insulin sensitivity across other metabolic organs including liver and skeletal muscle. The mechanism(s) and the quantitative improvements in insulin sensitivity across tissues with loss of adipocyte FAM20C is an outstanding question that will be the subject of future research. Overall, our data not only validate *Fam20c* as a key mediator of insulin resistance in adipocytes but also suggest that inhibition of *Fam20c* may serve as a promising therapeutic approach to alleviate obesity-induced metabolic dysfunction.

One striking finding from this study was a marked reduction in visceral WAT mass in iAd-Fam20c KO mice, coupled with a shift in adipocyte size distribution towards smaller adipocytes. Visceral WAT is a critical depot in obesity-associated metabolic diseases, as it is particularly susceptible to inflammatory expansion and dysfunction (54). Our results suggest that Fam20c plays a pivotal role in regulating visceral WAT expansion in response to obesity. The reduction in visceral WAT mass, despite no changes in subcutaneous or brown adipose tissue, suggests a potential depot-specific role of Fam20c in mediating adipose dysfunction. Moreover, this effect was not attributable to the degree of deletion, as all three depots displayed significant knockout. Further mechanistic studies are needed to elucidate the pathways by which Fam20c selectively impairs obesity-associated visceral WAT expansion. The shift toward smaller adipocytes in the absence of Fam20c likely reflects reduced adipocyte hypertrophy, which may limit the severity of visceral WAT dysfunction typically observed in obesity. Obesity is

frequently linked to increased basal lipolysis and attenuated catecholamine-stimulated lipolysis (39-41). In our study, visceral WAT from Ad-Fam20c KO mice exhibited lower basal lipolysis, with no alteration in stimulated lipolysis. This phenotype may be attributed to either enhanced insulin sensitivity in the adipose tissue or a direct modulation of the adipocyte triglyceride lipase PNPLA2 activity. Our phosphoproteomic analysis identified FAM20C-dependent phosphorylation of PNPLA2 at Ser468, suggesting a potential regulatory role of FAM20C in lipolysis. Further studies are required to elucidate the functional implications of this phosphorylation event and its broader effects on lipid metabolism.

Our phosphoproteomic analysis identified several putative FAM20C targets, both intracellular and secreted, highlighting its multifaceted role in adipocyte dysfunction. We observed FAM20C-dependent phosphorylation of CNPY4 at Ser64, which appears critical for amplifying inflammatory responses within adipocytes. Overexpression of wild-type CNPY4 enhanced proinflammatory cytokine production and impaired insulin sensitivity whereas its phosphorylation-deficient mutant (S64A) did not. This provides a direct mechanistic link between FAM20C kinase activity and adipocyte dysfunction, positioning CNPY4 as a downstream effector of FAM20C. Furthermore, we report an obesity-associated, isoform-specific change in *Cnpy4* expression in visceral WAT, with isoform 2 being selectively induced, suggesting that post-transcriptional regulation of *Cnpy4* may further shape inflammatory and metabolic outputs in obesity. Future in vivo studies are needed to define the role of CNPY4 in insulin resistance and adipose inflammation. While our findings elucidate one pathway of FAM20C-mediated dysfunction, they raise important questions about the breadth of its substrate specificity and the interplay

between intracellular and secreted phosphoproteins. Intracellularly, FAM20C-dependent phosphorylation of other substrates, such as SLC38A10, could regulate adipocyte amino acid transport to modulate inflammation and insulin sensitivity. Extracellularly, FAM20C-dependent phosphorylation of ECM components such as FN1 and LAMA4 suggests a broader role in tissue remodeling, fibrosis, and chronic inflammation, hallmarks of visceral WAT dysfunction. Further investigation into these pathways could reveal additional mechanisms through which FAM20C exacerbates metabolic disease.

Previous studies in liver (HepG2), breast cancer (MDA-MB-231), and osteosarcoma (U-2 OS) cell lines demonstrated that FAM20C is a critical regulator of the phosphosecretome (21). However, in our adipocyte secretome data, only a few secreted proteins were phosphorylated by FAM20C, indicating a cell-type specific effect. Prior work also showed that FAM20C phosphorylates plasma proteins, although these studies were conducted in vitro using conditioned media from cancer cell line models (21). Additional phosphoproteomic analyses of plasma are needed to identify FAM20C substrates in circulation. Furthermore, studies employing the ER-TurboID tag in Ad-Fam20c KO mice are essential to assess how adipocyte FAM20C contributes to the phosphorylation of plasma proteins. These investigations will help elucidate the mechanisms through which FAM20C might alter the plasma phosphoproteome, potentially exerting autocrine or paracrine effects that influence whole-body insulin sensitivity.

Our study also provides important clinical insights into the relationship between high adipose *FAM20C* expression and insulin resistance. There is pronounced heterogeneity in cardiometabolic risk among individuals with obesity, and those with MUO are known to exhibit altered gene expression in metabolic tissues including adipose and

skeletal muscle (30-32, 44). Peterson et. al. reported decreased expression of genes involved in inflammation and ECM remodeling in SC AT from MUO individuals (31), but it did not examine VIS AT. Utilizing a single-nuclei RNA-Seq study of VIS AT, we found that visceral adipocyte FAM20C is markedly elevated in MUO (44). In our study, FAM20C expression was markedly higher in VIS AT compared to SC AT, and its levels positively correlated with insulin resistance markers such as HOMA-IR and FPI. These correlations were particularly strong in individuals not receiving glucose-lowering medications, suggesting that FAM20C is not merely a consequence of metabolic dysregulation but a contributing factor. The preferential association of VIS AT FAM20C with metabolic impairment aligns with the notion that VIS AT is more metabolically active and inflammation-prone than SC AT, which has a protective role in energy storage. These data validate the translational relevance of our findings and highlight FAM20C as a potential biomarker for identifying individuals with obesity at high risk for T2D. Further studies measuring adipose and plasma levels of FAM20C in larger longitudinal cohorts of control and obese individuals are needed to validate these observations. Overall, our findings pave the way for the development of targeted therapies that modulate FAM20C activity in adipocytes to treat obesity-related metabolic diseases. Future research will be crucial to further elucidate the precise molecular targets of FAM20C in adipocytes and to translate these findings into effective therapies for metabolic diseases.

580

581

582

583

584

585

586

587

588

589

590

591

592

593

594

595

596

597

598

599

Materials and Methods

Experimental model and study participant details

Sex as a biological variable. Only male mice were used in the study since we observed spontaneous Cre activation and body weight changes in female *Fam20c-flox/Adiponectin-CreERT* mice in the absence of tamoxifen. To avoid confounding results, we precluded use of female mice.

In vivo Animal studies. All animal studies were approved by the Institutional Animal Care and Use Committee at Weill Cornell Medical College. Fam20c-floxed mice were a gift from Chunlin Qin's group (23) and backcrossed at least 5 generations to C57BL/6J mice. Adiponectin-Cre (strain#: 028020), Adiponectin-CreERT (strain#: 024671), and ob/ob (Strain#: 000632) mice were purchased from The Jackson Laboratory. Constitutive and conditional (tamoxifen inducible) adipocyte-specific Fam20c KO mice were generated by breeding Fam20c-floxed homozygous mice with Adiponectin-Cre and Adiponectin-CreERT mice respectively. Fam20c-floxed mice were used as controls from the same backcross generation. All mice were maintained in plastic cages under a 12-hour light/12-hour dark cycle at 22°C with free access to water and food (Control Diet: PicoLab Rodent Diet #5053, 20% protein, 4.5% fat). For the diet-induced obesity model, 4-week-old male and female mice were placed on a 60% HFD (D12492i, Research Diets) for respective time periods. Tamoxifen was dissolved in corn oil and injected intraperitoneally at 75 mg/kg/day. Fat and lean mass were determined via EchoMRI.

Studies involving human participants: Human data were sourced from the Leipzig Obesity Biobank (LOBB; https://www.helmholtz-munich.de/en/hi-mag/cohort/leipzig-

obesity-bio-bank-lobb). This biobank includes paired samples of abdominal subcutaneous and omental visceral adipose tissue, body fluids, and anthropometric data. Adipose samples were collected during elective laparoscopic surgeries following established protocols (55). Body composition and metabolic parameters were assessed using standardized methods (32, 56). The study was approved by the Ethics Committee of the University of Leipzig (approval no: 159-12-21052012) and conducted in accordance with the Declaration of Helsinki. All participants provided written informed consent. Exclusion criteria included age <18, chronic substance or alcohol misuse, smoking within the 12 months, acute inflammatory diseases, glitazone use, end-stage malignancy, >3% weight loss within three months, uncontrolled thyroid disorders, and Cushing's disease. The cross-sectional cohort comprised 1,480 individuals, divided into non-obese (N = 31; 52% female; age: 55.8 ± 13.4 years; BMI: 25.7 ± 2.7 kg/m²) and obese (N = 1,449; 72% female; age: 46.4 ± 11.7 years; BMI: 49.2 ± 8.3 kg/m²) groups. A smaller subset of this cohort was analyzed excluding those receiving blood glucose-lowering medications (insulin, metformin, DPP4 inhibitors, glitazones, or sulfonylureas). This sub-cohort included 203 individuals categorized into non-obese (N = 6; 34% female; age: 47.4 ± 5.7 years; BMI: $25.5 \pm 2.9 \text{ kg/m}^2$) and obese (N = 197; 68% female; age: $45.8 \pm 12.0 \text{ years}$; BMI: $48.5 \pm 7.6 \text{ kg/m}^2$). Cell lines and primary cultures. For primary differentiated adipocytes, stromal vascular fraction from inguinal adipose of 6-8-week-old male mice was prepared and differentiated for 6-8 days (57). Primary white adipocytes were cultured in DMEM/F12K media (Gibco, Thermo Fisher Scientific) with 10% FBS at 37°C, 5% CO₂, until confluent. Differentiation

622

623

624

625

626

627

628

629

630

631

632

633

634

635

636

637

638

639

640

641

642

643

644

involved 48-hour treatment with 0.5 mM 3-isobutyl-1-methylxanthine (IBMX), 1 mM

dexamethasone, 850 nM insulin, and 1 mM rosiglitazone, followed by 48 hours with 850 nM insulin and 1 mM rosiglitazone, then a further 48 hours with 850 nM insulin. For differentiated 3T3-L1 adipocytes, NIH/3T3 (ATCC, CRL-1658) fibroblasts were grown to 80% confluency and differentiated using the same protocol. To produce lentivirus, HEK-293T (ATCC, CRL-3216) cell line was used.

Method details

Blood chemistry and serum insulin analysis. Mice were fasted overnight (14–16 hours) for glucose tolerance tests and injected intraperitoneally with D-glucose solution (2g/kg). For insulin tolerance tests, mice were fasted for 6 hours and injected with 0.5 mlU/kg insulin. Blood glucose was measured by commercial glucometer (OneTouch) using tail-vein blood samples. Plasma insulin levels were measured after 6 h fasting. Blood was collected into lithium heparin tubes, centrifuged at 2000×g at 4°C, and plasma insulin levels were determined by ELISA (Mercodia). Plasma free fatty acids (FFA) were quantified using the NEFA-HR(2) assay kit (Fujifilm).

Histological analysis. Adipose tissue was immediately perfused with PBS and fixed with 10% neutral-buffered formalin (VWR), then transferred to 70% ethanol. Paraffinembedding, sectioning, and H&E staining were done by the MSKCC Laboratory of Comparative Pathology core facility. Slides were imaged using a Zeiss Axioscan7 at 20x magnification. Adipocyte diameter was measured from H&E-stained Visceral WAT sections using ImageJ (NIH) with Adiposoft plugin (58). For immunohistochemistry analysis of crown-like structures (CLS), tissue sections were incubated with anti-MAC-2 (Biolegend, 125402) followed by biotinylated and HRP-conjugated rat secondary antibody (Thermo, 31830). Histochemical reactions were performed using Vectastain ABC HRP Kit

(Vector Labs, PK-4000) and DAB peroxidase substrate kit (Vector Labs, SK-4100). Sections were counterstained with hematoxylin. CLS frequency was calculated as total number of CLS per 10,000 adipocytes.

Viral constructs and transduction. Adenoviral (pAd/CMV/V5-DEST™, #V49320, Invitrogen), retroviral (pMSCVpuro, #634401, Clontech), and lentiviral (pCDH-CMV-MCS-EF1-puro, #CD510B-1, System Biosciences) expression vectors were used. Mouse Fam20c and Cnpy4 CDS genes were cloned into these constructs. To generate Fam20c D473A and Cnpy4 S64A mutants, Quickchange II (200555, Agilent) site-directed mutagenesis kit was used. For viral production, packaging cells (Phoenix for retrovirus and 293T for lentivirus) were transfected at 70% confluence by lipofectamine 2000 (Invitrogen) method with 10μg of respective vectors. After 48 hours, the viral supernatant was harvested and filtered. Cells were incubated overnight with the viral supernatant, supplemented with 8 μg/ml polybrene. Subsequently, puromycin (Thermo Fisher) was used for selection.

RNA extraction and real-time quantitative PCR. Total RNA from adipose and adipocytes was isolated using the RNeasy Mini Kit (QIAGEN). A total of 1 μ g RNA was reverse-transcribed using high-capacity cDNA RT kit (Thermo Fisher). Quantitative PCR was performed using SYBR Green Master Mix (Quanta) and gene specific primers on the QuantStudio 6 Flex system (Thermo Fisher). Relative mRNA levels were determined by normalizing to ribosomal protein S18 (Rps18) using the $\Delta\Delta$ CT method. Primer sequences are listed in the supplemental table.

In vitro insulin sensitivity assay

Primary differentiated adipocytes were washed with PBS and incubated overnight in serum-free low-glucose DMEM with 0.5% BSA. Cells were stimulated with either 0 or 10nM insulin for 10 minutes. Media was removed and cells lysed with RIPA buffer for protein extraction and western blot analysis.

In vivo insulin sensitivity assay

Mice were fasted for 4 hours, injected with either PBS or 5 U/kg insulin intraperitoneally, and sacrificed 10 minutes post-injection. Adipose tissues, liver, and skeletal muscle were harvested for assessment of p-Akt and Akt protein by western blotting.

Flow Cytometry

Epididymal (visceral) adipose tissue was digested for 20 min in buffer containing collagenase D, Dispase-II, DNase-I, and calcium chloride. Cell suspensions were filtered through 100 μm then 40 μm filters, and the SVF was collected by centrifugation at 500 g for 10 min. Cells were incubated with CD16/32 (Fc block, Biolegend, 101302) for 15mins. Cells were then stained with anti-CD45.2 (Biolegend, 109824) for hematopoietic cells, anti-F4/80 (Biolegend, 123110) for macrophages, anti-CD11b (Biolegend, 101206) for macrophages, anti-CD19 (Biolegend, 115520) for B-cells, anti-CD4 (BD Biosciences, 553650) and anti-CD8 (BD Biosciences, 553032) for T-cells. DAPI stain (Biolegend, 422801) was used to mark dead cells. Cells were analyzed using a Sony MA900 cell sorter and FlowJo software.

Western blot analysis

- Cells or tissues were lysed in RIPA buffer with protease and phosphatase inhibitors.
- Protein extracts were resolved on NuPAGE Bis-Tris (Thermo) gels and transferred to

PVDF membranes. Membranes were incubated overnight (4 °C) with primary antibodies including FAM20C (Proteintech, 25395-I-AP), p-AKT Ser473 (Cell Signaling, 9271S), AKT (Cell Signaling, 9272S), CNPY4 (AF5015, R&D Systems), and Actin-HRP (Life Technologies, MA515739HRP). Detection of proteins was carried out by incubations with HRP-conjugated secondary antibodies followed by enhanced chemiluminescence detection reagents. Band intensity was quantified using Fiji/ImageJ (NIH)

Unbiased Transcriptomics. Unbiased transcriptomic analyses of whole visceral WAT, adipocyte fraction, SVF, and primary differentiated adipocytes transduced with adenovirus was performed using the Affymetrix GeneChip Mouse Genome 430A 2.0 Array (Thermo Fisher) using manufacturer's protocol.

RNA Sequencing and pathway analysis. After RNA isolation, RNA integrity was analyzed using an Agilent 2100-Bioanalyzer, and concentrations measured by NanoDrop (Thermo Fisher). Preparation of RNA library was performed by the Genomics Core at Weill Cornell Medicine using the SMARTer v4 Ultra Low Input RNA Kit (Clontech, #63488) and Nextera XT DNA Library Preparation Kit (Illumina, San Diego, CA). The normalized cDNA libraries were pooled and sequenced on an Illumina HiSeq4000 sequencer at 50 pair-end cycles. Sequencing reads were mapped with STAR v2.6.0c to the mouse reference genome (GRCm38.p6) (59). Fragments per gene were counted with featureCounts v1.6.2 with respect to Ensembl annotations 33137190. Differentially expressed genes between pairwise comparisons were identified by Wald tests using DESeq2 v1.26.080, with Benjamini–Hochberg corrected two-tailed p-values < 0.05 considered statistically significant (60). Biological analyses, including canonical pathways, biological processes or transcription factors were performed using the

Ingenuity Pathway Analysis (Qiagen). Base-2 log-transformed counts per million (CPM) values were used for heatmap plots of bulk RNA-seq data, which were centered and scaled by row.

Proteomic Sample Preparation and LC-MS³ Analysis

Intracellular and secretome phosphoproteomic sample preparation was conducted as previously described (61). Detailed methodology for phosphoproteomic experiments can be found in supplemental methods.

Human Adipose RNA sequencing. RNA was extracted from adipose tissue using the SMART-seq protocol (62). Single-end sequencing of all libraries was performed on Novaseq 6000 at the Functional Genomics Center Zurich. The raw sequencing reads underwent adapter and quality trimming with Fastp v0.20.0 (63), applying a minimum read length of 18 nucleotides and a quality threshold of 20. Read alignment to the human reference genome (assembly GRCh38.p13, GENCODE release 32) and gene-level expression quantification were executed using Kallisto v0.48 (64). Samples with read counts >20 million were down-sampled to this threshold using ezRun v3.14.1 (https://github.com/uzh/ezRun, accessed on March 23, 2022). Data normalization was performed using a weighted trimmed mean (TMM) of the log expression ratios, with adjustments made for age, sex, and transcript integrity numbers (TINs). All analyses were carried out in R v4.3.1 (www.R-project.org).

Statistical Analysis

All statistical analyses were performed using GraphPad Prism 9. Unpaired 2-tailed t tests, unpaired Welch's t test, and 2-way ANOVA were used. P < 0.05 was considered

statistically significant. All data were assessed for normality and found to be normally distributed to support the application of parametric statistical tests. Data in bar graphs indicate mean±SEM. Details on individual statistical tests and number of samples (N) are indicated in respective figure legends.

Study Approval

All animal studies were approved by the Institutional Animal Care and Use Committee and Research Animal Resource Center at Weill Cornell Medical College. The human study received ethical approval from the Ethics Committee of the University of Leipzig (approval no: 159-12-21052012) and was conducted in accordance with the principles outlined in the Declaration of Helsinki. All participants provided written informed consent before being included in the study.

Data and materials availability

The main data supporting the findings of this study are available within the article and its supplemental files, including the Supporting Data Values. The human RNA-seq data from the LOBB have not been deposited in a public repository due to restrictions imposed by patient consent but can be obtained from Matthias Blüher upon request. Mouse RNA-Seq data will be made available in Geo with accession numbers once the databases are operational following the end of the government shutdown. All derived MS/MS data and metadata are made publicly available on MassIVE (Accession: MSV000099484) and ProteomeXchange (Accession: PXD069449).

Author contributions:

Conceptualization: AG, JCL

- Methodology: AG, JCL, BS, AH, BB, OE, EH, LM, ARN, TT, RL, EEH, GJAC
- 780 Investigation: AG, EAH, LM, ARN, TT, RL, EEH
- 781 Visualization: AG, JCL, BS, AH
- Funding acquisition: AG, JCL, EAH, EEH, MB
- 783 Project administration: AG, JCL
- 784 Supervision: AG, JCL
- 785 Writing original draft: AG, JCL
- 786 Writing review & editing: AG, BS, EAH, LM, ARN, TT, RL, BB, OE, AH, AG, FN, CW, MB
- 787 **Acknowledgements:** We thank Wenfei Sun and Hua Dong for supporting human
- adipose tissue RNA-seq. The graphical renderings were created with BioRender.com. We
- thank Bruce Spiegelman for helpful discussions on the project. The views expressed in
- this manuscript are those of the authors and do not necessarily represent the official views
- of the American Diabetes Association, the National Institute of Diabetes and Digestive
- and Kidney Diseases, the National Institute of Allergy and Infectious Diseases, or the
- 793 National Institutes of Health.

794 Funding:

- This work is the result of NIH funding, in whole or in part, and is subject to the NIH Public
- Access Policy. Through acceptance of this federal funding, the NIH has been given a right
- to make the work publicly available in PubMed Central.
- National Institutes of Health (NIH) grants R01 DK121140 and R01 DK121844 (JCL)

| 799 | American Diabetes Association postdoctoral fellowship 9-22-PDFPM-01 (AG) |
|-----|--|
| 800 | Tri-I StARR – NIAID Fellowship 1-R38-AI174255-01 (EEH) |
| 801 | American Heart Association postdoctoral fellowship 23DIVSUP1074485 (RL) |
| 802 | NIH postdoctoral fellowship T32-HL160520 (EAH) |
| 803 | German Research Foundation grant 209933838, SFB 1052 (project B1) (MB) |
| 804 | Deutsches Zentrum für Diabetesforschung grant 82DZD00601 (MB) |
| 805 | |
| 806 | |
| 807 | |
| 808 | |

References

809

- 1. Barnes AS. The epidemic of obesity and diabetes: trends and treatments. *Tex*
- 811 *Heart Inst J.* 2011;38(2):142-4.
- 812 2. Bhupathiraju SN, and Hu FB. Epidemiology of Obesity and Diabetes and Their
- Cardiovascular Complications. *Circ Res.* 2016;118(11):1723-35.
- S14 3. Chew NWS, Ng CH, Tan DJH, Kong G, Lin C, Chin YH, et al. The global burden of
- metabolic disease: Data from 2000 to 2019. *Cell Metab.* 2023;35(3):414-28 e3.
- 816 4. Bluher M. Obesity: global epidemiology and pathogenesis. *Nat Rev Endocrinol*.
- 817 2019;15(5):288-98.
- 818 5. Roden M, and Shulman GI. The integrative biology of type 2 diabetes. *Nature*.
- 2019;576(7785):51-60.
- 820 6. Rosen ED, and Spiegelman BM. What we talk about when we talk about fat. *Cell*.
- 821 2014;156(1-2):20-44.
- 822 7. Gilani A, Stoll L, Homan EA, and Lo JC. Adipose Signals Regulating Distal Organ
- Health and Disease. *Diabetes*. 2024;73(2):169-77.
- 824 8. Czech MP. Mechanisms of insulin resistance related to white, beige, and brown
- 825 adipocytes. *Mol Metab.* 2020;34:27-42.
- 826 9. Klein S, Gastaldelli A, Yki-Jarvinen H, and Scherer PE. Why does obesity cause
- 827 diabetes? *Cell Metab.* 2022;34(1):11-20.
- 828 10. Saltiel AR, and Olefsky JM. Inflammatory mechanisms linking obesity and
- metabolic disease. *J Clin Invest.* 2017;127(1):1-4.
- 830 11. Savage DB, Petersen KF, and Shulman GI. Disordered lipid metabolism and the
- pathogenesis of insulin resistance. *Physiol Rev.* 2007;87(2):507-20.

- Hildebrandt X, Ibrahim M, and Peltzer N. Cell death and inflammation during obesity: "Know my methods, WAT(son)". *Cell Death Differ.* 2023;30(2):279-92.
- 834 13. Rosen ED, and Kajimura S. Is it time to rethink the relationship between adipose
- inflammation and insulin resistance? Journal of Clinical Investigation.
- 836 2024;134(17).
- 837 14. Kahn CR, Wang GX, and Lee KY. Altered adipose tissue and adipocyte function in
- the pathogenesis of metabolic syndrome. Journal of Clinical Investigation.
- 839 2019;129(10):3990-4000.
- 840 15. Nicolás G-B, Guseh JS, Ge L, Alfonso R-N, Tong C, Bre Anne P, et al. Adipsin
- preserves beta cells in diabetic mice and associates with protection from type 2
- diabetes in humans. *Nature medicine*. 2019;25:1739.
- 843 16. Solinas G, and Becattini B. JNK at the crossroad of obesity, insulin resistance, and
- cell stress response. *Molecular Metabolism*. 2017;6(2).
- 845 17. Zhao P, Wong KI, Sun XL, Reilly SM, Uhm M, Liao ZJ, et al. TBK1 at the
- Crossroads of Inflammation and Energy Homeostasis in Adipose Tissue. *Cell.*
- 847 2018;172(4):731-+.
- 848 18. Reilly SM, and Saltiel AR. Adapting to obesity with adipose tissue inflammation.
- 849 Nat Rev Endocrinol. 2017;13(11):633-43.
- 850 19. Reilly SM, Chiang SH, Decker SJ, Chang L, Uhm M, Larsen MJ, et al. An inhibitor
- of the protein kinases TBK1 and IKK-varepsilon improves obesity-related
- metabolic dysfunctions in mice. *Nat Med.* 2013;19(3):313-21.

- 20. Tagliabracci VS, Engel JL, Wen JZ, Wiley SE, Worby CA, Kinch LN, et al. Secreted
- Kinase Phosphorylates Extracellular Proteins That Regulate Biomineralization.
- 855 *Science*. 2012;336(6085):1150-3.
- Tagliabracci VS, Wiley SE, Guo X, Kinch LN, Durrant E, Wen J, et al. A Single
- Kinase Generates the Majority of the Secreted Phosphoproteome. Cell.
- 858 2015;161(7):1619-32.
- 859 22. Simpson MA, Hsu R, Keir LS, Hao J, Sivapalan G, Ernst LM, et al. Mutations in
- FAM20C are associated with lethal osteosclerotic bone dysplasia (Raine
- syndrome), highlighting a crucial molecule in bone development. *Am J Hum Genet*.
- 862 2007;81(5):906-12.
- 23. Liu P, Ma S, Zhang H, Liu C, Lu Y, Chen L, et al. Specific ablation of mouse
- Fam20C in cells expressing type I collagen leads to skeletal defects and
- hypophosphatemia. *Sci Rep.* 2017;7(1):3590.
- 866 24. Sriwattanapong K, Theerapanon T, Khamwachirapitak C, Sae-Ear P, Sa-Ard-Iam
- N, Shotelersuk V, et al. In-depth investigation of FAM20A insufficiency effects on
- deciduous dental pulp cells: Altered behaviours, osteogenic differentiation, and
- inflammatory gene expression. *Int Endod J.* 2024;57(6):745-58.
- 870 25. Liu X, Jiang L, Zhang W, Zhang J, Luan X, Zhan Y, et al. Fam20c regulates the
- calpain proteolysis system through phosphorylating Calpasatatin to maintain cell
- 872 homeostasis. *J Transl Med.* 2023;21(1):417.
- 26. Lin JH, Lin IP, Ohyama Y, Mochida H, Kudo A, Kaku M, et al. FAM20C directly
- binds to and phosphorylates Periostin. *Sci Rep.* 2020;10(1):17155.

- Da Q, Han H, Valladolid C, Fernandez M, Khatlani T, Pradhan S, et al. In vitro phosphorylation of von Willebrand factor by FAM20c enhances its ability to support platelet adhesion. *J Thromb Haemost*. 2019;17(6):866-77.
- Hecht TK, Blank B, Steger M, Lopez V, Beck G, Ramazanov B, et al. Fam20C regulates protein secretion by Cab45 phosphorylation. *J Cell Biol.* 2020;219(6).
- 880 29. Ben Djoudi Ouadda A, Gauthier MS, Susan-Resiga D, Girard E, Essalmani R,
 881 Black M, et al. Ser-Phosphorylation of PCSK9 (Proprotein Convertase Subtilisin882 Kexin 9) by Fam20C (Family With Sequence Similarity 20, Member C) Kinase
 883 Enhances Its Ability to Degrade the LDLR (Low-Density Lipoprotein Receptor).
 884 Arterioscler Thromb Vasc Biol. 2019;39(10):1996-2013.
- Schulze MB, and Stefan N. Metabolically healthy obesity: from epidemiology and mechanisms to clinical implications. *Nat Rev Endocrinol.* 2024;20(11):633-46.
- Petersen MC, Smith GI, Palacios HH, Farabi SS, Yoshino M, Yoshino J, et al.

 Cardiometabolic characteristics of people with metabolically healthy and unhealthy

 obesity. *Cell Metab.* 2024;36(4):745-61 e5.
- 890 32. Bluher M. Metabolically Healthy Obesity. Endocr Rev. 2020;41(3).
- Wang X, Wang S, Li C, Gao T, Liu Y, Rangiani A, et al. Inactivation of a novel FGF23 regulator, FAM20C, leads to hypophosphatemic rickets in mice. *PLoS Genet*. 2012;8(5):e1002708.
- 894 34. Emont MP, Jacobs C, Essene AL, Pant D, Tenen D, Colleluori G, et al. A single-895 cell atlas of human and mouse white adipose tissue. *Nature*. 2022;603(7903):926-896 33.

- 897 35. Feng WC, Ting Y, Tang X, Liu D, Zhou WC, Li YK, et al. The role of ESM1 in the
- lipids metabolic reprogramming and angiogenesis of lung adenocarcinoma cells.
- 899 *Heliyon.* 2024;10(17).
- 900 36. Janke J, Engeli S, Gorzelniak K, Feldpausch M, Heintze U, Böhnke J, et al.
- Adipose tissue and circulating endothelial cell specific molecule-1 in human
- 902 obesity. *Horm Metab Res.* 2006;38(1):28-33.
- 903 37. Kleiner S, Mepani RJ, Laznik D, Ye L, Jurczak MJ, Jornayvaz FR, et al.
- Development of insulin resistance in mice lacking PGC-1α in adipose tissues.
- Proceedings of the National Academy of Sciences of the United States of America.
- 906 2012;109(24):9635-40.
- 907 38. Stromsdorfer KL, Yamaguchi S, Yoon MJ, Moseley AC, Franczyk MP, Kelly SC, et
- 908 al. NAMPT-Mediated NAD
- 909 Biosynthesis in Adipocytes Regulates Adipose Tissue Function and Multi-organ Insulin
- 910 Sensitivity in Mice. *Cell Rep.* 2016;16(7):1851-60.
- 911 39. Gaidhu MP, Anthony NM, Patel P, Hawke TJ, and Ceddia RB. Dysregulation of
- lipolysis and lipid metabolism in visceral and subcutaneous adipocytes by high-fat
- diet: role of ATGL, HSL, and AMPK. Am J Physiol Cell Physiol. 2010;298(4):C961-
- 914 71.
- 915 40. Valentine JM, Ahmadian M, Keinan O, Abu-Odeh M, Zhao P, Zhou X, et al. beta3-
- Adrenergic receptor downregulation leads to adipocyte catecholamine resistance
- 917 in obesity. *J Clin Invest.* 2022;132(2).

- 918 41. Reynisdottir S, Langin D, Carlstrom K, Holm C, Rossner S, and Arner P. Effects of 919 weight reduction on the regulation of lipolysis in adipocytes of women with upper-920 body obesity. *Clin Sci (Lond)*. 1995;89(4):421-9.
- 42. Lu YC, Yeh WC, and Ohashi PS. LPS/TLR4 signal transduction pathway. *Cytokine*.
 2008;42(2):145-51.
- 923 43. Konno K, Wakabayashi Y, Akashi-Takamura S, Ishii T, Kobayashi M, Takahashi K,
 924 et al. A molecule that is associated with Toll-like receptor 4 and regulates its cell
 925 surface expression. *Biochem Biophys Res Commun.* 2006;339(4):1076-82.
- 926 44. Reinisch I, Ghosh A, Noe F, Sun W, Dong H, Leary P, et al. Unveiling adipose 927 populations linked to metabolic health in obesity. *Cell Metab.* 2025;37(3):640-55 928 e4.
- 929 45. Vijay J, Gauthier MF, Biswell RL, Louiselle DA, Johnston JJ, Cheung WA, et al.
 930 Single-cell analysis of human adipose tissue identifies depot and disease specific
 931 cell types. *Nat Metab.* 2020;2(1):97-109.
- 932 46. An JX, Wang Q, Yi SQ, Liu XM, Jin H, Xu JY, et al. The source of the fat significantly 933 affects the results of high-fat diet intervention. *Sci Rep-Uk.* 2022;12(1).
- Lang P, Hasselwander S, Li H, and Xia N. Effects of different diets used in diet induced obesity models on insulin resistance and vascular dysfunction in C57BL/6
 mice. Sci Rep. 2019;9(1):19556.
- Hernandez ED, Lee SJ, Kim JY, Duran A, Linares JF, Yajima T, et al. A macrophage
 NBR1-MEKK3 complex triggers JNK-mediated adipose tissue inflammation in
 obesity. *Cell Metab.* 2014;20(3):499-511.

- 49. Hotamisligil GS, Shargill NS, and Spiegelman BM. Adipose expression of tumor
 941 necrosis factor-alpha: direct role in obesity-linked insulin resistance. *Science*.
 942 1993;259(5091):87-91.
- 943 50. Han MS, White A, Perry RJ, Camporez JP, Hidalgo J, Shulman GI, et al. Regulation 944 of adipose tissue inflammation by interleukin 6. *Proc Natl Acad Sci U S A*. 945 2020;117(6):2751-60.
- Choi MJ, Jung SB, Lee SE, Kang SG, Lee JH, Ryu MJ, et al. An adipocyte-specific defect in oxidative phosphorylation increases systemic energy expenditure and protects against diet-induced obesity in mouse models. *Diabetologia*. 2020;63(4):837-52.
- 950 52. Masschelin PM, Cox AR, Chernis N, and Hartig SM. The Impact of Oxidative Stress 951 on Adipose Tissue Energy Balance. *Front Physiol.* 2019;10:1638.
- Deng L, Huang Y, Zhao F, Chen P, and Huang X. Lack of adipocyte FAM20C improves whole body glucose homeostasis. *Physiol Rep.* 2024;12(21):e70126.
- 954 54. Sakers A, De Siqueira MK, Seale P, and Villanueva CJ. Adipose-tissue plasticity in 955 health and disease. *Cell.* 2022;185(3):419-46.
- 55. Langhardt J, Flehmig G, Kloting N, Lehmann S, Ebert T, Kern M, et al. Effects of
 Weight Loss on Glutathione Peroxidase 3 Serum Concentrations and Adipose
 Tissue Expression in Human Obesity. *Obes Facts*. 2018;11(6):475-90.
- Kloting N, Fasshauer M, Dietrich A, Kovacs P, Schon MR, Kern M, et al. Insulin sensitive obesity. *Am J Physiol Endocrinol Metab*. 2010;299(3):E506-15.

- 57. Kajimura S, Seale P, Kubota K, Lunsford E, Frangioni JV, Gygi SP, et al. Initiation
- of myoblast to brown fat switch by a PRDM16-C/EBP-beta transcriptional complex.
- 963 *Nature*. 2009;460(7259):1154-8.
- 58. Galarraga M. Adiposoft: An automated software for the analysis of white adipose
- tissue cellularity in histological sections (vol 53, pg 2791, 2012). J Lipid Res.
- 966 2014;55(12):2705-.
- 967 59. Dobin A, Davis CA, Schlesinger F, Drenkow J, Zaleski C, Jha S, et al. STAR:
- ultrafast universal RNA-seq aligner. *Bioinformatics*. 2013;29(1):15-21.
- 969 60. Love MI, Huber W, and Anders S. Moderated estimation of fold change and
- dispersion for RNA-seq data with DESeq2. *Genome Biol.* 2014;15(12):550.
- 971 61. Stein BD, Ferrarone JR, Gardner EE, Chang JW, Wu D, Hollstein PE, et al. LKB1-
- Dependent Regulation of TPI1 Creates a Divergent Metabolic Liability between
- Human and Mouse Lung Adenocarcinoma. *Cancer Discov.* 2023;13(4):1002-25.
- 974 62. Picelli S, Faridani OR, Bjorklund AK, Winberg G, Sagasser S, and Sandberg R.
- Full-length RNA-seq from single cells using Smart-seq2. *Nat Protoc.*
- 976 2014;9(1):171-81.
- 977 63. Chen S, Zhou Y, Chen Y, and Gu J. fastp: an ultra-fast all-in-one FASTQ
- 978 preprocessor. *Bioinformatics*. 2018;34(17):i884-i90.
- 979 64. Bray NL, Pimentel H, Melsted P, and Pachter L. Near-optimal probabilistic RNA-
- seq quantification (vol 34, pg 525, 2016). *Nat Biotechnol.* 2016;34(8):888-.

Figure Legends

Figure 1. FAM20C is an obesity-induced serine threonine kinase in adipocytes. (A) Schematic of visceral WAT collection from diet-induced obesity (DIO) model of B6/J mice and its fractionation into adipocyte and stromal vascular compartments. (B) Volcano plot of DEGs from whole adipose tissue (C) adipocyte fraction, and (D) stromal vascular fractions of High-fat diet (HFD) versus Control Diet (CD) fed B6/J mice. (E) Relative mRNA expression of proinflammatory genes in primary adipocytes of B6/J transduced with respective viral constructs (n=3 per group). (F) Schematic of mouse FAM20C protein with highlighted key domains and catalytic site (G) Fam20c mRNA expression from visceral white adipose tissue (WAT) of CD and HFD fed B6/J mice at respective time points (n=4 per group). (H) Fam20c mRNA expression from visceral WAT of 6-week-old WT B6/J and leptin deficient ob/ob mice on CD (n=5 per group). *p<0.05, **p<0.01 by unpaired Student's t-test.

Figure 2. Induction of adipocyte Fam20c elicits a proinflammatory gene expression signature. (A) Schematic of viral transduction of primary differentiated adipocytes with respective constructs. (B) Relative mRNA expression of proinflammatory genes in primary adipocytes transduced with respective viral constructs (n=4 per group). (C) Heatmap of DEGs in primary adipocytes transduced with respective viral constructs (n=4 per group). (D) Hallmark Pathway Analysis of top DEG between Fam20c WT and Fam20c D473A (kinase dead mutant) groups. (E) Representative western blot images and (F) quantification for insulin mediated p-Akt S473 induction in primary adipocytes transduced with respective viral constructs and stimulated with either PBS or insulin (10nM for 10min) (n=4 per group). A total of three independent experiments were performed. (G) Heatmap

of differentially expressed genes (DEG) in primary differentiated adipocytes from control and Ad-Fam20c KO mice (n=4 per group). (H) Hallmark Pathway analysis of DEG between primary differentiated adipocytes from control and Ad-Fam20c KO mice. (I) Upstream Analysis showing top activated and inactivated pathways and (J) upstream cytokine pathways based on DEG in primary differentiated adipocytes from control and Ad-Fam20c KO mice. An activation Z-score of ≥2 was used as cutoff. *p<0.05, **p<0.01, ****p<0.001, ****p<0.0001 by two-way ANOVA followed by Bonferroni multiple comparison's test for B and by One-way ANOVA for F.

1007

1008

1009

1010

1011

1012

1013

1014

1015

1016

1017

1018

1019

1020

1021

1022

1023

1024

1025

1026

1027

1028

1029

Figure 3: Adipocyte-specific deletion of Fam20c corrects metabolic impairments of diet-induced obesity. (A) Schematic of mouse models employing acute (2 weeks) and chronic (12 weeks) knockout of adipocyte Fam20c as a disease modifying therapy for obesity induced T2D. (B) Body weights at different time points, (C) Glucose tolerance test (GTT), and (E) Insulin tolerance test (ITT) for control and iAd-Fam20c KO mice following acute deletion of adipocyte Fam20c (n=11 per group). (D) and (F) represent Area Under Curve calculations for C and E, respectively. (G) Body weights at different time points, (H) Glucose tolerance test, and (J) Insulin tolerance test for control and iAd-Fam20c KO mice following chronic deletion of adipocyte Fam20c (n=10 per group). (I) and (K) represent Area Under Curve calculations for H and J, respectively. (L) Adipose tissue insulin resistance index (Adipo-IR) as a marker of adipose insulin sensitivity, (M) Body composition analysis by EchoMRI, and (N) Fat mass to lean mass ratio from HFD-fed control and iAd-Fam20c KO mice following chronic Fam20c deletion (n=6 per group). (O) Mass of adipose tissue depots and liver from HFD-fed control and iAd-Fam20c KO mice following chronic Fam20c deletion (n=10 per group). *p<0.05, **p<0.01, ***p<0.001 by unpaired Student's t-test for D, F, I, K, L, M, N, and O. Repeated Measures Two-way ANOVA for C, E, H, and J.

1030

1031

1032

1033

1034

1035

1036

1037

1038

1039

1040

1041

1042

1043

1044

1045

1046

1047

1048

1049

1050

1051

Figure 4: Adipocyte-specific deletion of Fam20c shifts adipocyte size distribution towards smaller adipocytes, decreases adipose tissue macrophages, and improves insulin sensitivity. (A) Representative images of Hematoxylin and Eosinstained visceral WAT sections of HFD-fed control and iAd-Fam20c KO mice following chronic Fam20c deletion. Scale bar, 100 µm. (B) Mean adipocyte diameter and (C) Frequency size distribution for adipocyte size in HFD-fed control and iAd-Fam20c KO mice following chronic Fam20c deletion (n=6 per group). (D) Number of adipose tissue macrophages (F4/80+CD11b+), B-cells (CD19+), CD4+, and CD8+ cells in control and iAd-Fam20c KO mice fed HFD for 4 weeks followed by acute Fam20c deletion (n=4-6 per group). (E) Representative images of Mac-2-staining, (F) Quantification of Macrophage (Mac-2 stained) area represented as % of total adipose area, and (G) quantification of crown-like structures (CLS) represented as CLS per 10,000 adipocytes from visceral WAT sections of control and iAd-Fam20c KO mice fed HFD for 4 weeks followed by acute Fam20c deletion (n=4 per group). (H) Representative western blot images for insulin mediated p-Akt stimulation in subcutaneous and visceral WAT of control and iAd-Fam20c KO mice fed HFD for 4 weeks followed by acute Fam20c deletion. (I) AND (J) Quantifications for p-Akt/Akt from H for subcutaneous and visceral WAT, respectively (n=4 per group). (K) Representative western blot images for insulin mediated p-Akt stimulation in liver and skeletal muscle of control and iAd-Fam20c KO mice fed HFD for 4 weeks followed by acute Fam20c deletion. (L) and (M) Quantifications for p-Akt/Akt from K for liver and skeletal muscle, respectively. *p<0.05, **p<0.01, ****p<0.0001 by unpaired Student's t-test.

Figure 5: Adipocyte FAM20C phosphorylates a distinct set of intracellular proteins.

(A) Schematic for LC-MS/MS based unbiased phosphoproteomic analysis of intracellular proteins from primary differentiated adipocytes transduced with respective viral constructs. (B) Heatmap showing top differentially phosphorylated proteins in primary adipocytes transduced with respective viral constructs. (C) Motif Analysis and Sitemap of top identified FAM20C dependent phosphosites in B. (D) Pathway Analysis of differentially expressed phosphopeptides from primary adipocytes transduced with either a WT construct of Fam20c or a kinase dead mutant (D473A).

Figure 6: Adipocyte FAM20C phosphorylates a distinct set of secreted proteins. (A) Schematic for LC-MS/MS based unbiased phosphoproteomic analysis of secreted proteins from control and Fam20c deficient primary adipocytes. (B) Volcano plot showing top differentially phosphorylated secreted proteins in primary adipocytes with and without Fam20c. (C) Motif Analysis and Sitemap of top identified FAM20C-dependent phosphosites in B. (D) Pathway Analysis of differentially expressed secreted phosphoproteins in primary adipocytes with and without Fam20c. (E) FFA release plotted over time and (F) Rate of FFA production per hour from VAT explants of HFD-fed control and Ad-Fam20c KO mice treated with either vehicle or 0.5μM CL-316243 (n=6 per group). (G) Glycerol release plotted over time and (H) Rate of glycerol production per hour from VAT explants of HFD-fed control and Ad-Fam20c KO mice treated with either vehicle or 0.5μM CL-316243 (n=6 per group). *p<0.05 by two-way ANOVA followed by Sidak's post-hoc multiple comparison test.

Figure 7: Obesity-induced FAM20C in the visceral WAT phosphorylates proteins causing adipose tissue dysfunction. (A) Schematic of LC-MS/MS based unbiased phosphoproteomic analysis of visceral WAT from HFD-fed control and Ad-Fam20c KO mice. (B) Volcano plot showing top differentially phosphorylated proteins in visceral WAT of control versus Ad-Fam20c KO mice. (C) Motif Analysis and Sitemap of top identified FAM20C dependent phosphosites in B. (D) Relative expression of mouse Cnpy4 transcript variant 1 (Cnpy4-1), transcript variant 2 (Cnpy4-2), and transcript variant 3 (Cnpy4-3) in B6 WT mice fed either a CD or HFD for 12 weeks (n=5 per group). (E) Relative mRNA expression of proinflammatory genes in primary adipocytes transduced with respective viral constructs (n=4 per group). (F) Representative western blot images and (G) quantification for insulin mediated p-Akt S473 induction in primary adipocytes transduced with respective viral constructs and stimulated with either PBS or insulin (10nM for 10min) (n=4 per group). A total of three independent experiments were conducted. *p<0.05, **p<0.01, ***p<0.001, ****p<0.0001 Student's t-test for D, Two-way ANOVA for E and One-way ANOVA for G.

1075

1076

1077

1078

1079

1080

1081

1082

1083

1084

1085

1086

1087

1088

1089

1090

1091

1092

1093

1094

1095

1096

1097

Figure 8: Adipose FAM20C expression in humans positively correlates with insulin resistance. (A) FAM20C gene expression comparison for subcutaneous (SC) and visceral (VIS) adipose tissues for patient subgroups with and without obesity. (B) FAM20C gene correlation analysis with metabolic parameters. (C) Correlation of SC FAM20C gene expression with HOMA-IR (D) Correlation of VIS FAM20C gene expression with HOMA-IR (E) Correlation of SC FAM20C gene expression with FPI (F) Correlation of VIS FAM20C gene expression with FPI (G) Correlation of SC FAM20C gene expression with BMI for body weight for males (H) Correlation of VIS FAM20C gene expression with BMI for

males. (I) Correlation of VIS FAM20C gene expression with HOMA-IR in individuals not receiving antihyperglycemic medications. (J) Correlation of VIS FAM20C gene expression with FPI in individuals not receiving antihyperglycemic medications. (K) Visceral adipocyte FAM20C expression from single-nuclei RNA sequencing study in metabolically healthy obese (MHO) and metabolically unhealthy obese (MUO) individuals. FPI: Fasting Plasma Insulin; HOMA-IR: Homeostasis Model Assessment of Insulin Resistance; *p<0.05, **p<0.01, ***p<0.01 Welch's one way ANOVA with Games-Howell post-hoc Test for A, Spearman correlation coefficient analysis with a confidence interval of 0.95 for B-J, Student's t-test for K.

Figure 1

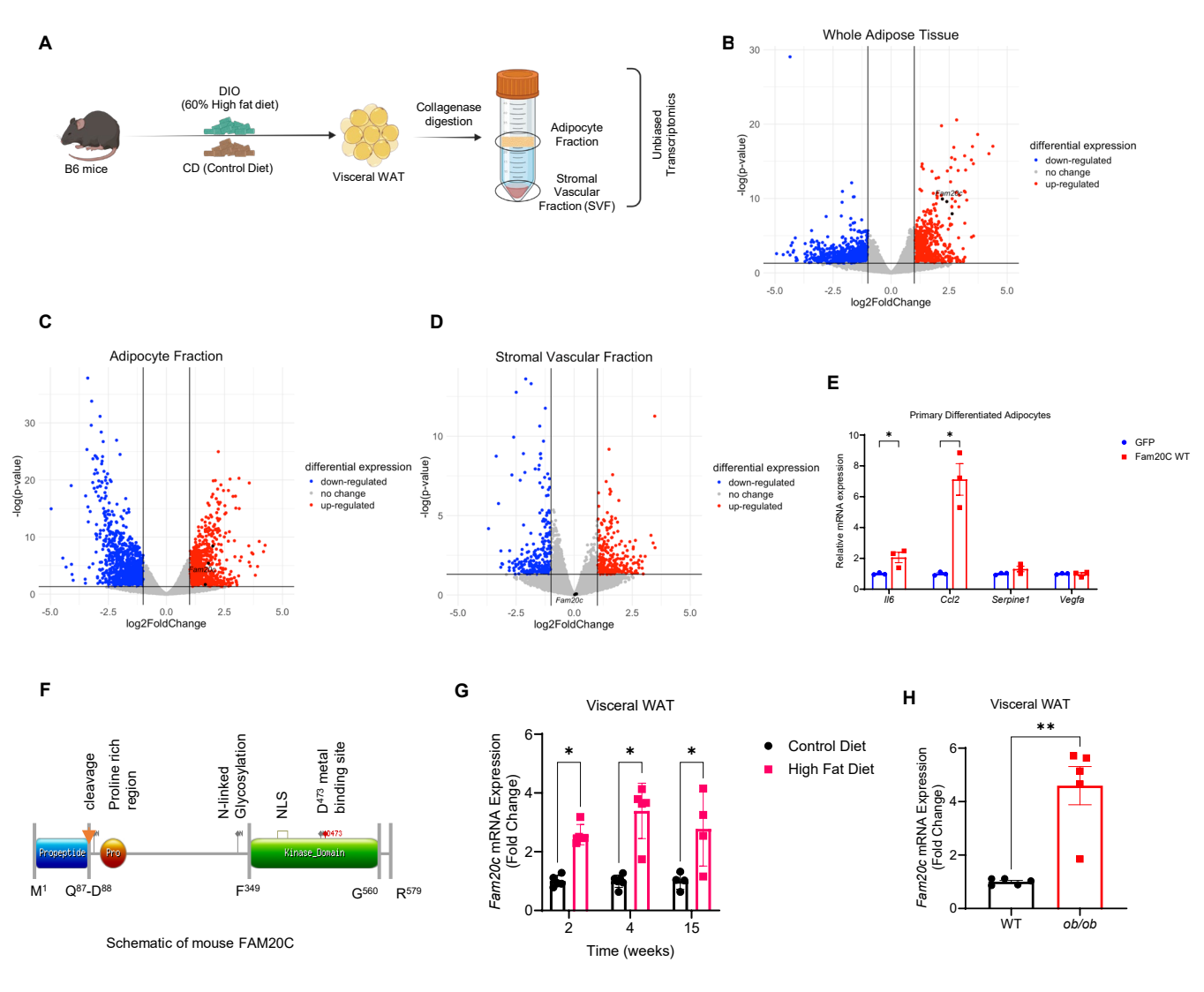


Figure 2

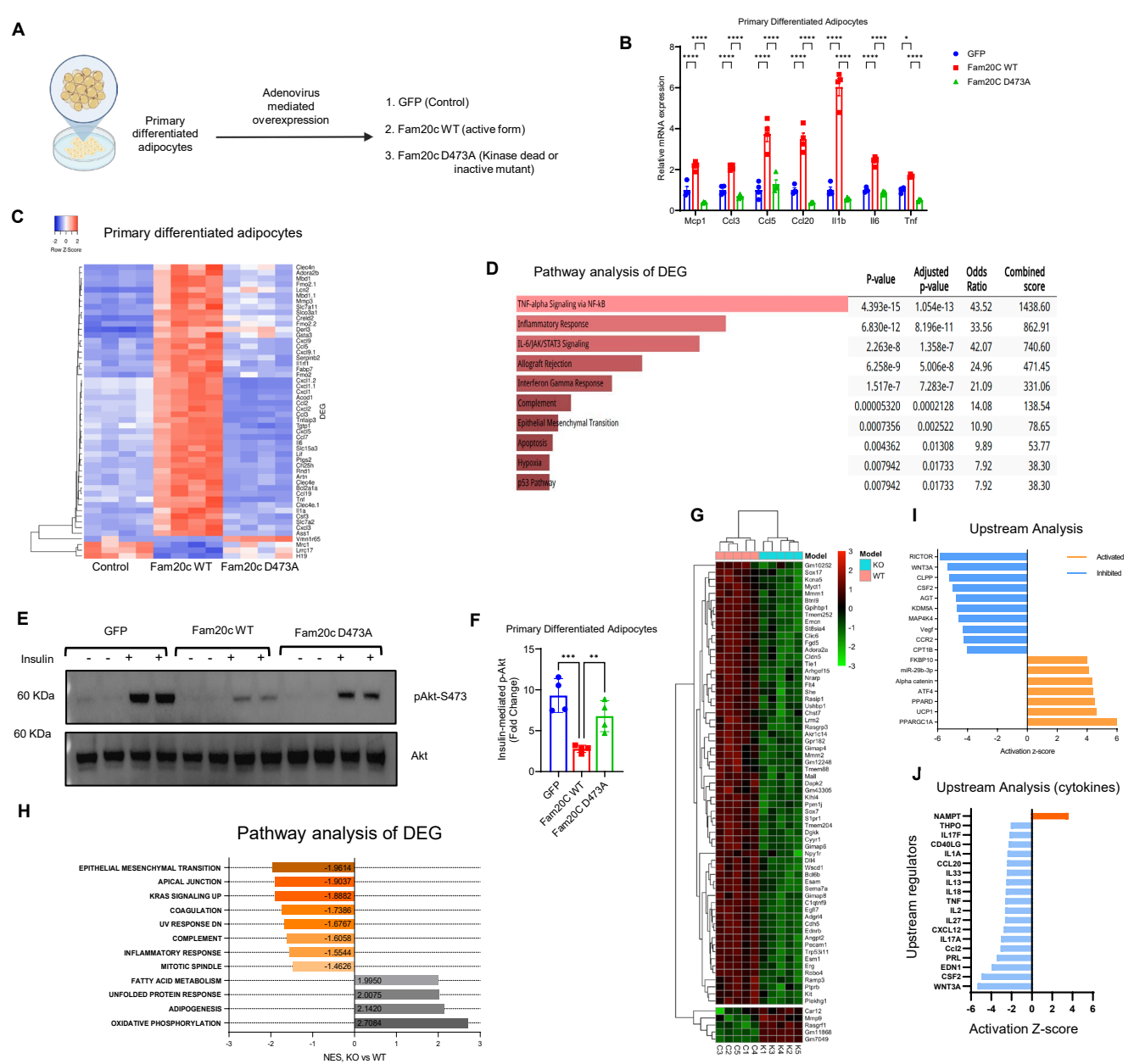


Figure 3

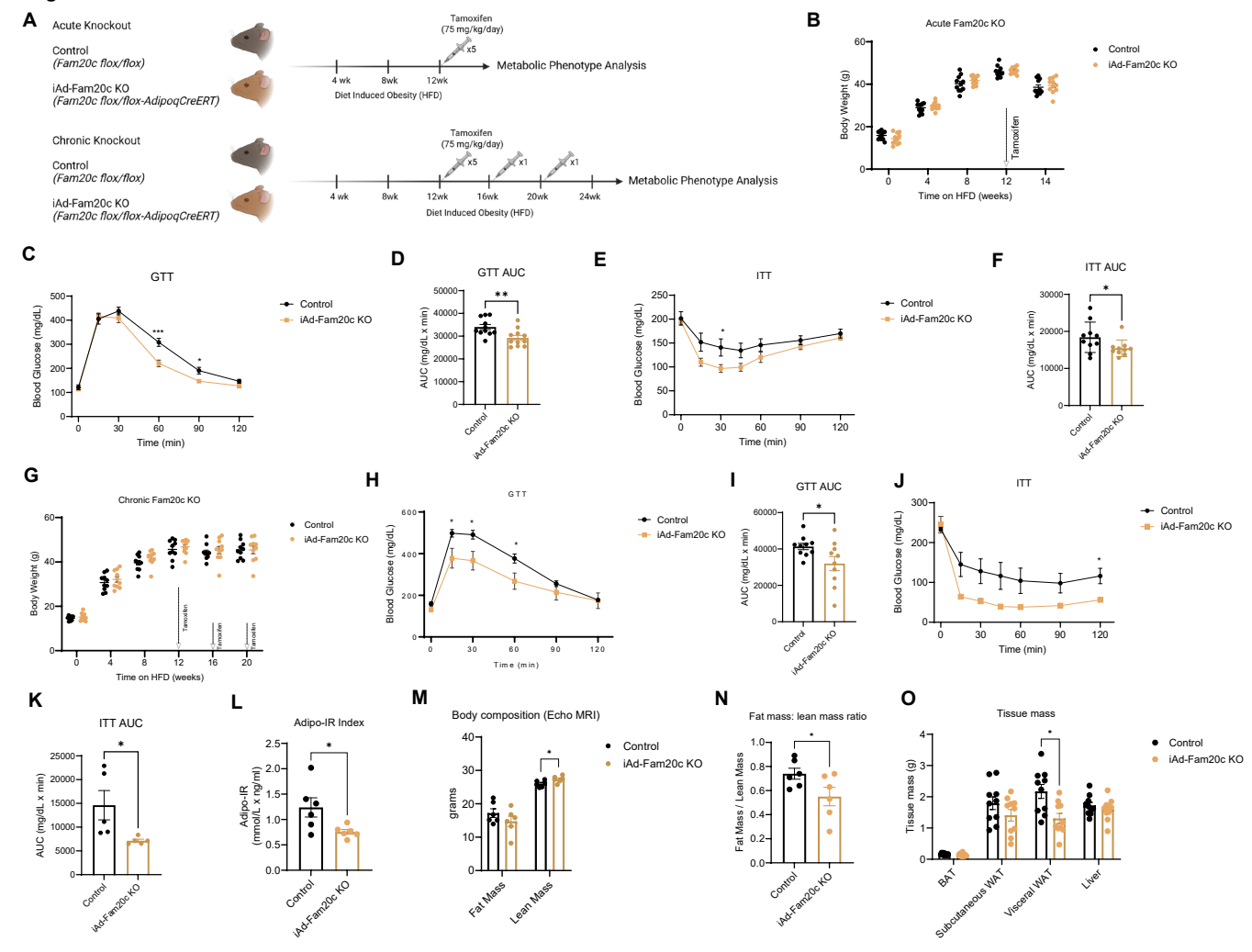


Figure 4

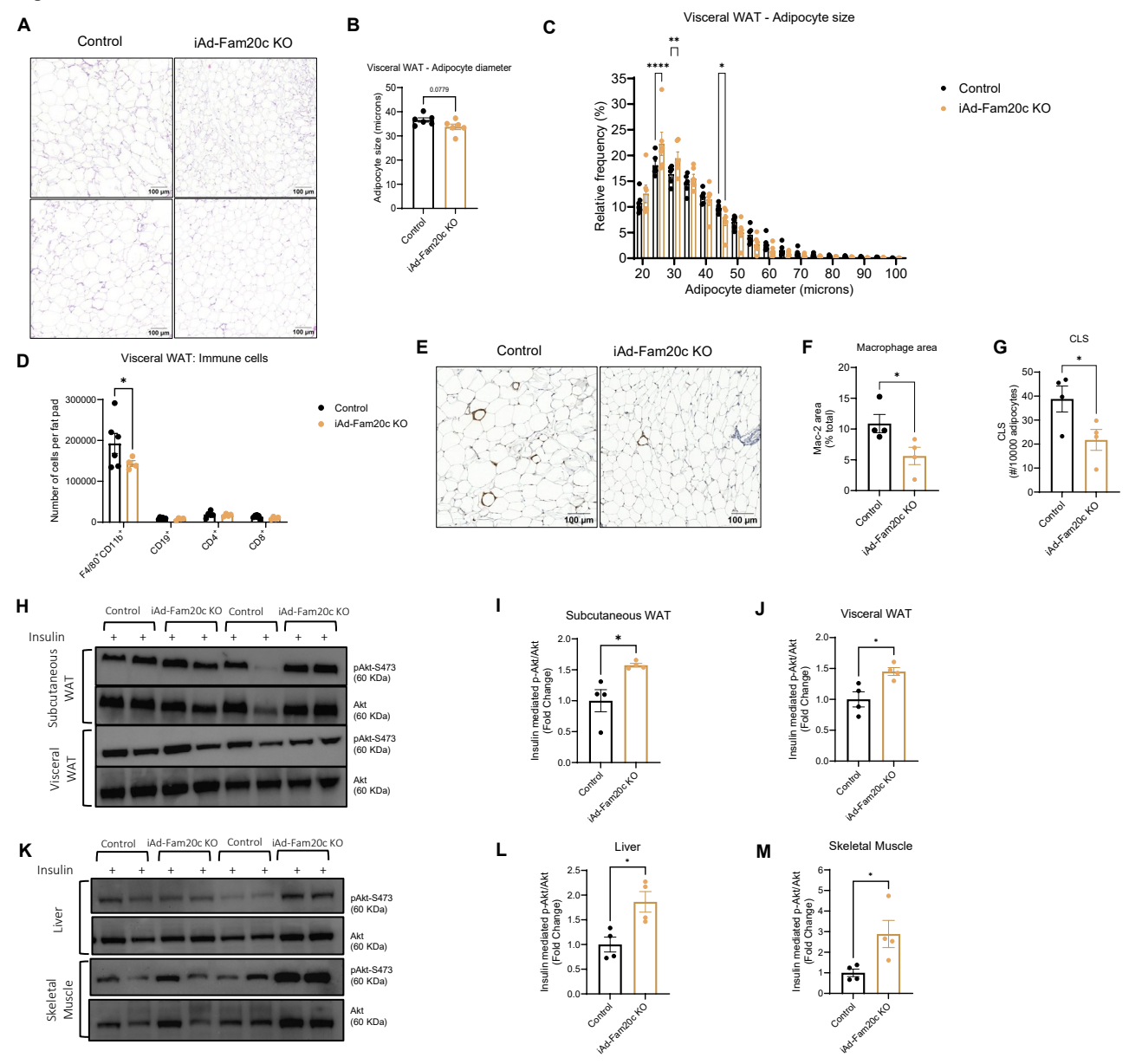
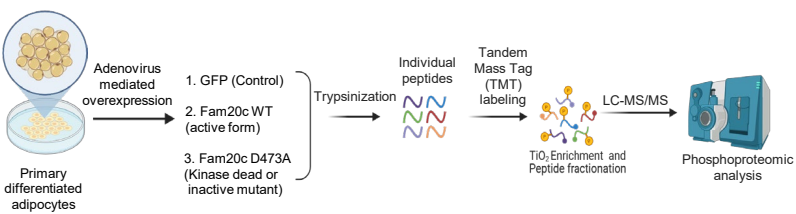
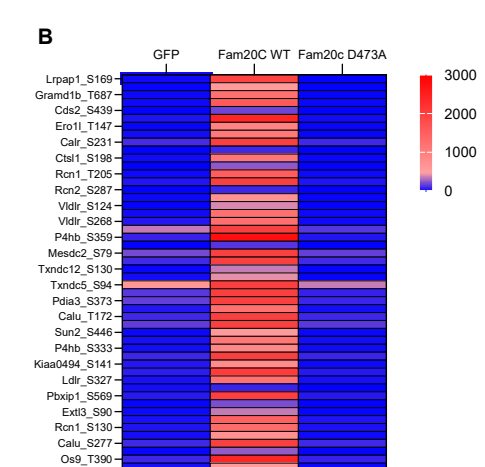


Figure 5





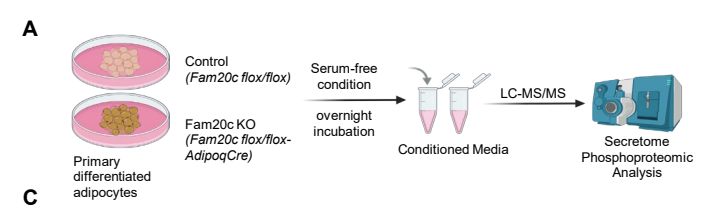


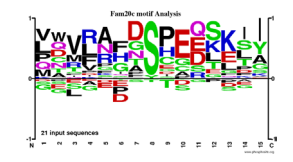


D Pathway Analysis of differentially expressed phosphopeptides

| | P-value | Adjusted p-value | Odds Ratio | Combined score |
|--|-----------|---------------------|---------------|----------------|
| Focal Adhesion WP85 | 0.0001184 | 0.006370 | 4.26 | 38.48 |
| Comprehensive IL 17A Signaling WP5242 | 0.0001654 | 0.006370 | 5.63 | 49.06 |
| Inflammatory Response Pathway WP458 | 0.001012 | 0.02422 | 10.19 | 70.27 |
| Focal Adhesion PI3K Akt mTOR Signaling Pathway WP2841 | 0.001258 | 0.02422 | 2.83 | 18.92 |
| Fatty Acid Beta Oxidation WP1269 | 0.001634 | 0.02484 | 8.83 | 56.66 |
| Endochondral Ossification WP1270 | 0.002232 | 0.02484 | 5.93 | 36.17 |
| G Protein Signaling Pathways WP232 | 0.002259 | 0.02484 | 4.81 | 29.29 |
| <u> </u> | 0.003155 | 0.03037 | 5.44 | 31.32 |
| Alpha 6 Beta 4 Integrin Signaling Pathway WP488 | 0.003589 | 0.03071 | 6.97 | 39.23 |
| Splicing Factor NOVA Regulated Synaptic Proteins WP1983 | 0.003309 | 0.03071 | 0.57 | 33.23 |
| Dysregular ed miRNA Targeting In Insulin PI3K AKT Signaling WP3855 | 0.006791 | 0.05049 | 8.61 | 42.99 |

Figure 6

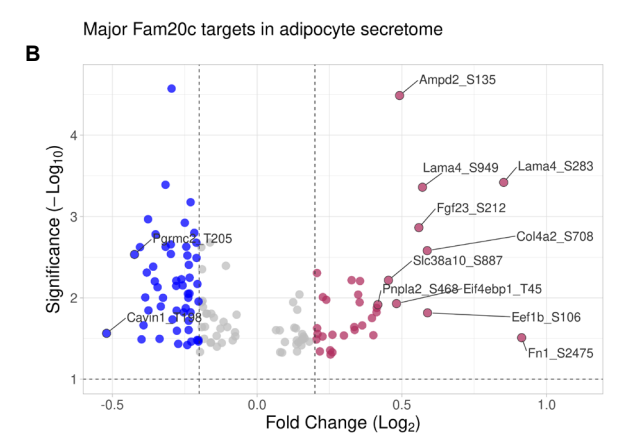


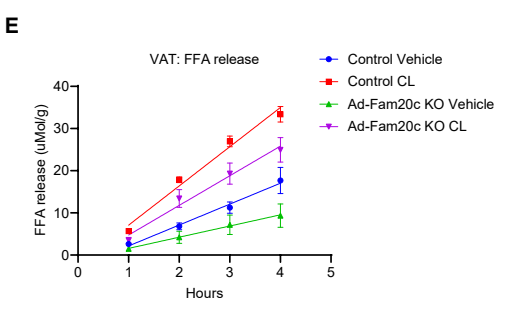


D Pathway Analysis of differentially expressed phosphopeptides

| | P-value | p-value | Ratio | score |
|--|-----------|---------|-------|--------|
| cal Adhesion WP85 | 0.0002843 | 0.01279 | 7.27 | 59.33 |
| ocal Adhesion PI3K Akt mTOR Signaling Pathway WP2841 | 0.0009787 | 0.02202 | 4.84 | 33.51 |
| pha 6 Beta 4 Integrin Signaling Pathway WP488 | 0.004057 | 0.06085 | 10.05 | 55.35 |
| mprehensive IL 17A Signaling WP5242 | 0.01379 | 0.1551 | 6.32 | 27.07 |
| anslation Factors WP307 | 0.02272 | 0.1828 | 9.09 | 34.39 |
| r 193A And MVP In Colon Cancer Metastasis WP3979 | 0.02875 | 0.1828 | 41.45 | 147.12 |
| l <mark>cium Regulatio</mark> n In Cardiac Cells WP553 | 0.03299 | 0.1828 | 4.47 | 15.26 |
| yometrial Relaxation And Contraction Pathways WP385 | 0.03596 | 0.1828 | 4.32 | 14.36 |
| egulation Of A <mark>ctin Cytoskeleton WP523</mark> | 0.03657 | 0.1828 | 4.29 | 14.19 |
| Isteoblast Signaling WP238 | 0.04747 | 0.2136 | 23.03 | 70.18 |

Adjusted Odds Combined





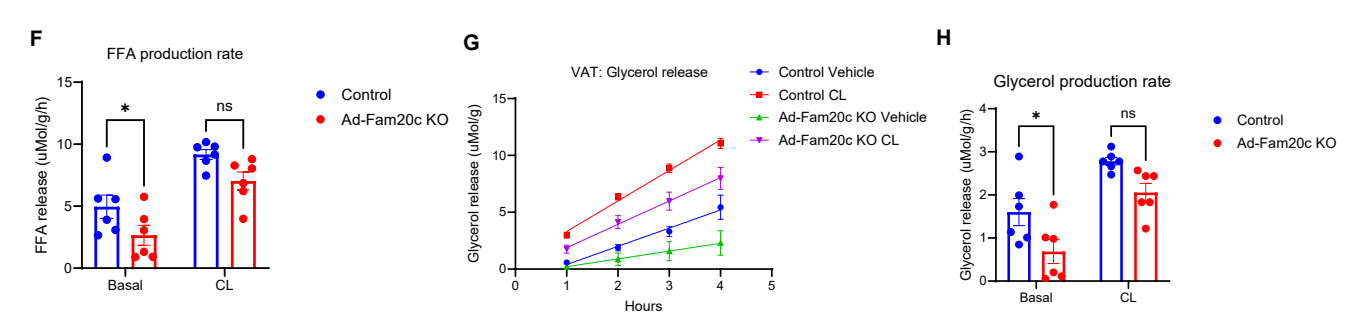


Figure 7

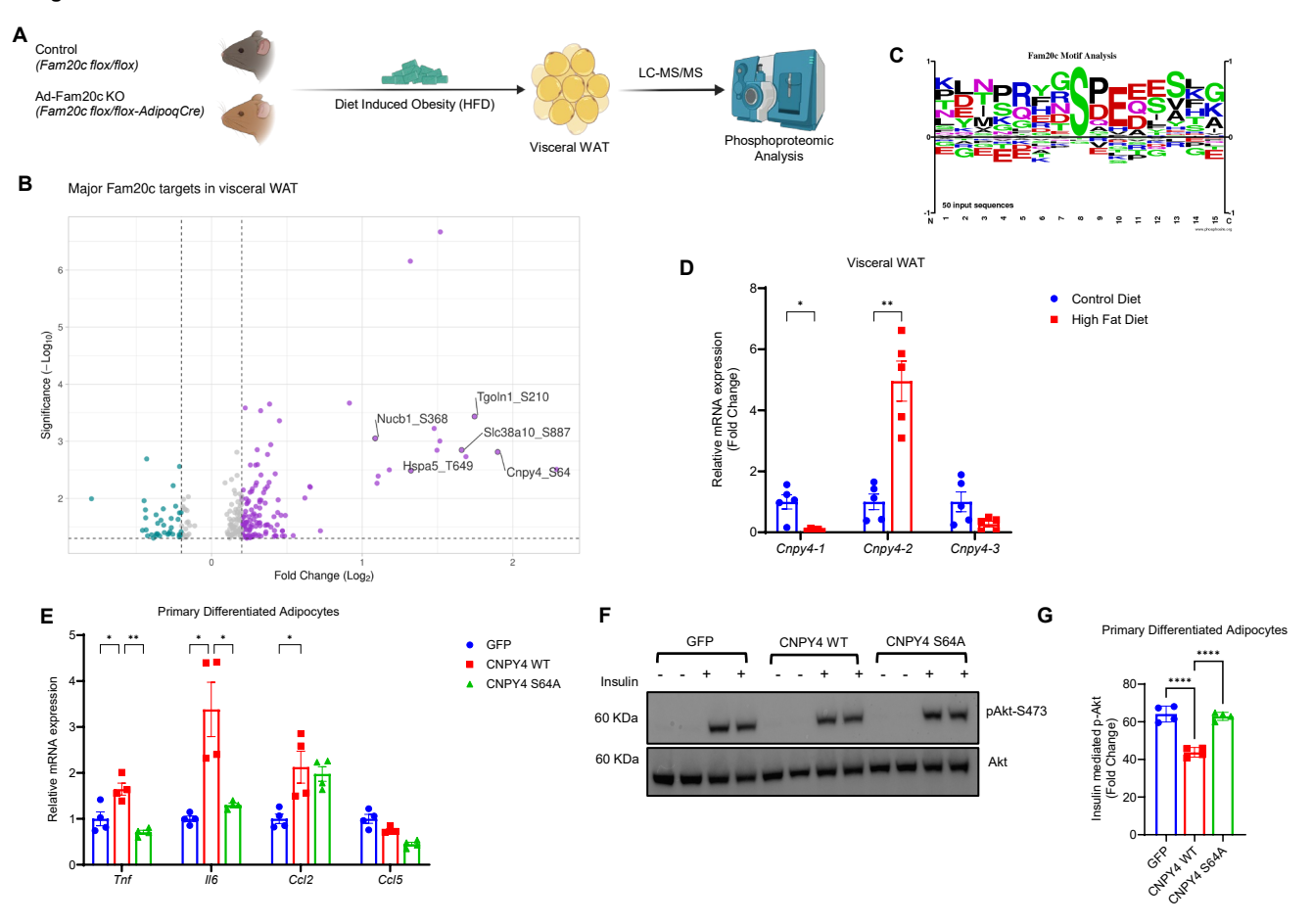


Figure 8

